

# Secondary organic material formed by methylglyoxal in aqueous aerosol mimics

N. Sareen, A. N. Schwier, E. L. Shapiro, D. Mitroo, and V. F. McNeill

Department of Chemical Engineering, Columbia University, New York, NY, USA

Received: 15 July 2009 – Published in Atmos. Chem. Phys. Discuss.: 24 July 2009

Revised: 13 January 2010 – Accepted: 14 January 2010 – Published: 1 February 2010

**Abstract.** We show that methylglyoxal forms light-absorbing secondary organic material in aqueous ammonium sulfate and ammonium nitrate solutions mimicking tropospheric aerosol particles. The kinetics were characterized using UV-Vis spectrophotometry. The results suggest that the bimolecular reaction of methylglyoxal with an ammonium or hydronium ion is the rate-limiting step for the formation of light-absorbing species, with  $k_{\text{NH}_4^+}^{\text{II}} = 5 \times 10^{-6} \text{ M}^{-1} \text{ min}^{-1}$  and  $k_{\text{H}_3\text{O}^+}^{\text{II}} \leq 10^{-3} \text{ M}^{-1} \text{ min}^{-1}$ . Evidence of aldol condensation products and oligomeric species up to 759 amu was found using chemical ionization mass spectrometry with a volatilization flow tube inlet (Aerosol-CIMS). Tentative identifications of carbon-nitrogen species and a sulfur-containing compound were also made using Aerosol-CIMS. Aqueous solutions of methylglyoxal, with and without inorganic salts, exhibit significant surface tension depression. These observations add to the growing body of evidence that dicarbonyl compounds may form secondary organic material in the aerosol aqueous phase, and that secondary organic aerosol formation via heterogeneous processes may affect seed aerosol properties.

## 1 Introduction

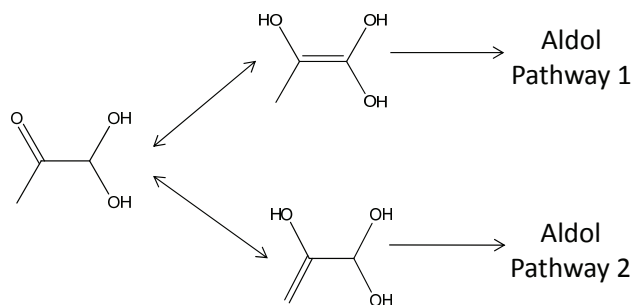
Laboratory and field studies suggest that carbonyl-containing volatile organic compounds, when absorbed by aqueous aerosol particles or cloud droplets, participate in aqueous-phase chemistry to form low-volatility secondary organic material (SOA) (Jang et al., 2002; Kroll et al., 2005; Ligio et al., 2005; Volkamer et al., 2006, 2007, 2009; Loeffler et al., 2006; Zhao et al., 2006; Gao et al., 2006; Altieri et al., 2008; Carlton et al., 2008; Nozière et al., 2009a, b; Gal-

loway et al., 2009; Shapiro et al., 2009; Fu et al., 2009; El Haddad et al., 2009; De Haan et al., 2009a). There is evidence that SOA formation may affect properties of the seed aerosol such as CCN activity (Cruz and Pandis, 1997; Hartz et al., 2005; King et al., 2007, 2009; Engelhart et al., 2008; Duplissy et al., 2008; Michaud et al., 2009), optical properties (Saathoff et al., 2003; Nozière et al., 2007, 2009b; Nozière and Esteve, 2007; Casale et al., 2007; Shapiro et al., 2009; De Haan et al., 2009a) and heterogeneous reactivity towards gases such as  $\text{N}_2\text{O}_5$  (Folkers et al., 2003; Anttila et al., 2006). A variety of potentially surface-active SOA products have been proposed, including organic acids, organosulfates, nitrogen-containing organics, aldol condensation products, and highly oxygenated oligomeric material. In an aqueous aerosol particle, surface-active products may partition to the gas-particle interface, lowering the surface tension (and thus the critical supersaturation required for cloud droplet activation) and acting as a barrier to mass transport between the gas and aqueous phases. Light-absorbing SOA products which could increase the absorption index of the seed aerosol have also been identified in laboratory studies. Aldehydes have been reported to undergo aldol condensation in aqueous aerosol mimics to form  $\pi$ -conjugated species (Nozière et al., 2007; Nozière and Esteve, 2007; Casale et al., 2007). We recently reported the formation of light-absorbing, oligomeric molecules in aqueous aerosol mimics containing glyoxal and ammonium salts (Shapiro et al., 2009). De Haan et al. (2009a, b) observed browning upon the reaction of glyoxal with amino acids in aerosol and cloud droplet mimics.

Methylglyoxal ( $\text{C}_3\text{H}_4\text{O}_2$ ) is an atmospheric oxidation product of many anthropogenic and biogenic volatile organic compounds (Tuazon et al., 1986; Grosjean et al., 1993; Smith et al., 1999). There is mixed evidence in the literature regarding the potential of methylglyoxal to be a direct precursor for heterogeneous SOA formation in aqueous aerosols. Methylglyoxal becomes hydrated and forms



Correspondence to: V. F. McNeill  
(vfm2103@columbia.edu)



**Scheme 1.** Proposed reaction pathways for methylglyoxal.

acetal and hemiacetal oligomers in aqueous solution (Nemet et al., 2004; Paulsen et al., 2005; Loeffler et al., 2006; Zhao et al., 2006; Krizner et al., 2009). Kalberer et al. (2004) suggested that methylglyoxal acetal oligomers could explain their observation of polymeric material in secondary organic aerosols formed in a reaction chamber by the photooxidation of 1,3,5-trimethylbenzene. Barsanti and Pankow (2005) and Krizner et al. (2009) predicted that aldol condensation should be favorable for methylglyoxal in aerosols. Singly hydrated methylglyoxal has been reported to be the dominant monomeric species in aqueous methylglyoxal systems (Nemet et al., 2004). Singly hydrated methylglyoxal may participate in self-aldol condensation via two possible pathways initiating with enol formation with the C=C double bond forming from either terminal carbon, as shown in Scheme 1. Note that we refer to the overall process of aldol addition followed by dehydration as aldol condensation (Muller, 1994). Zhao et al. (2006) measured non-zero methylglyoxal uptake onto aqueous sulfuric acid solutions in a coated-wall flow tube reactor. However, in aerosol chamber studies Kroll et al. (2005) observed that methylglyoxal uptake to acidic ammonium sulfate seed aerosols did not lead to significant particle growth.

We studied the formation of light-absorbing secondary organic products in aqueous solutions containing methylglyoxal and ammonium salts. The kinetics of formation were characterized using UV-Vis spectrophotometry. We also characterized the reaction products via atomization of diluted reaction mixtures followed by detection with chemical ionization mass spectrometry with a volatilization flow tube inlet (Aerosol-CIMS). We found evidence of aldol condensation products and high-molecular-weight oligomeric species, as well as possible sulfur-containing compounds and carbon-nitrogen species. Pendant drop tensiometry measurements show that aqueous solutions of methylglyoxal exhibit surface tension depression, and the effect is enhanced when NaCl or  $(\text{NH}_4)_2\text{SO}_4$  is present. These observations add to the growing body of evidence that dicarbonyl compounds form secondary organic material in the aqueous phase, and that SOA formation via heterogeneous processes may affect seed aerosol properties.

## 2 Methods

### 2.1 Bulk solution preparation

Salt concentrations in atmospheric aerosols at typical relative humidities exceed bulk saturation concentrations (Tang and Munkelwitz, 1994; Tang et al., 1997). In an effort to mimic atmospheric aerosol compositions to the extent possible in a bulk solution, solutions were prepared using Millipore water and high (near-saturation) concentrations of the salt of interest (3.1 M  $(\text{NH}_4)_2\text{SO}_4$ , 5.1 M NaCl, 1.18 M  $\text{Na}_2\text{SO}_4$ , 8.7 M  $\text{NH}_4\text{NO}_3$ ). Methylglyoxal concentrations ranged from 0–2.0 M, corresponding to ~0–25 wt% of the solute. Methylglyoxal was introduced from a 40 wt% aqueous solution (Sigma Aldrich). Mixing time was counted as time after the 40 wt% methylglyoxal solution was introduced to the aqueous salt solution. The aqueous methylglyoxal stock solution was pH=2.0 ( $\pm 0.1$ ) when tested with an Accumet model 20 pH/conductivity meter (Fisher Scientific), and the reaction mixtures that contained  $\geq 16.2$  mM methylglyoxal were pH=2.0 ( $\pm 0.1$ ), without buffering or further addition of acid. This is within the range of pH relevant to tropospheric aerosols (Keene et al., 2004; Zhang et al., 2007). In experiments performed to test the effect of varying pH, dilute  $\text{HNO}_3$  was added to the reaction mixtures dropwise until the desired pH was reached.

Methylglyoxal stock solution is acidic due to the presence of a small amount of pyruvic acid impurity. Pyruvic acid is a relatively strong organic acid, with  $\text{pK}_a=2.49$ . Therefore, the fact that our stock solution is pH=2 corresponds to a very small (0.07% by mole) impurity of pyruvic acid in the methylglyoxal stock solution.

Solutions were prepared in 100 mL Pyrex volumetric flasks. Pyrex is opaque to light with wavelengths  $<280$  nm (Corning, Inc.), but the samples were not further protected from ambient light except for control experiments as specified in the text. All experiments were performed at ambient temperature and pressure.

### 2.2 UV-Vis spectrophotometry

The UV-Vis absorption spectra of the reaction mixtures were measured using an HP 8453 UV-Visible Spectrophotometer with a 10 mm open-top quartz cuvette.

### 2.3 Surface tension measurements

Surface tension was measured using pendant drop tensiometry as described in Shapiro et al. (2009). Briefly, droplets of sample solution were suspended from the tip of a glass capillary tube using a 100  $\mu\text{L}$  syringe mounted inside a chamber with quartz windows. Images were captured as described by Anastasiadis et al. (1987). The method of Canny (1986) was

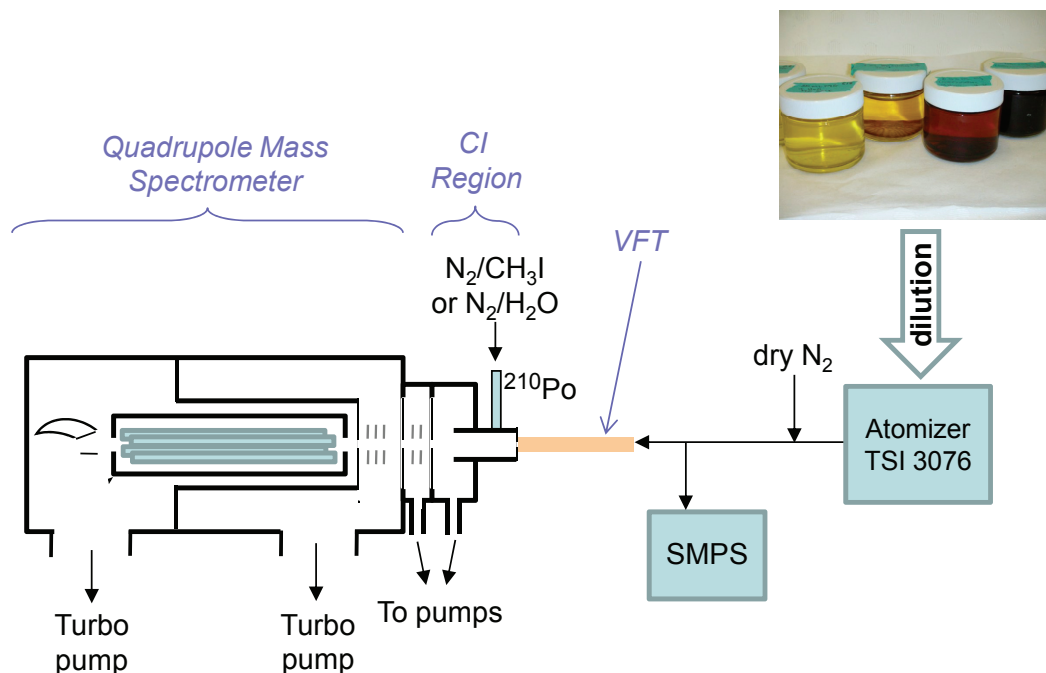


**Fig. 1.** Schematic of Aerosol-CIMS setup for the detection of products formed during the reactions of methylglyoxal in aqueous solution with  $(\text{NH}_4)_2\text{SO}_4$  or NaCl. SMPS: scanning mobility particle sizer, VFT: volatilization flow tube, CI: chemical ionization. See text for details.

implemented in MATLAB 7.0 (The MathWorks, Inc.) for edge detection. Surface tension was calculated according to:

$$\sigma = \frac{\Delta\rho g d_e^2}{H} \quad (1)$$

where  $\sigma$  is surface tension,  $\Delta\rho$  is the difference in density between the solution and the gas phase,  $g$  is acceleration due to gravity,  $d_e$  is the equatorial diameter of the droplet, and  $H$  is the shape factor (Adamson and Gast, 1997). The method of several selected planes was used for determining  $H$  based on the diameter of the drop at five intervals along the drop axis (Juza, 1997). Solution density was measured using an analytical balance readable to within  $\pm 10 \mu\text{g}$  (Denver Instruments).

## 2.4 Aerosol-CIMS

Aerosol-CIMS enables measurements of aerosol composition simultaneously with gas-phase composition, with the high sensitivity, selectivity, and fast time response of CIMS (Hearn and Smith, 2004a, 2006b; McNeill et al., 2007, 2008). This technique allows speciated measurements of aerosol organics which are selective based on the choice of parent ion. Chemical ionization is a relatively soft ionization technique that results in low fragmentation of organics, thus simplifying their identification and quantification. Aerosol-CIMS has been used for laboratory studies of the oxidative aging of organic aerosols (Hearn and Smith, 2004b,

2005, 2006a, 2007; Hearn et al., 2005, 2007; McNeill et al., 2007, 2008) and to characterize aerosols of unknown, complex chemical composition (Hearn and Smith, 2006b).

Experiments were conducted using a custom-built Aerosol-CIMS apparatus. Analyte molecules were detected as the products of their interactions with  $\text{I}^-$  or  $\text{H}_3\text{O}^+(\text{H}_2\text{O})_n$  using a quadrupole mass spectrometer with high mass ( $\leq 1000$  amu) capabilities (Extrel CMS). The two reagent ions used,  $\text{I}^-$  and  $\text{H}_3\text{O}^+(\text{H}_2\text{O})_n$ , are complementary in their versatility ( $\text{H}_3\text{O}^+(\text{H}_2\text{O})_n$ ) and selectivity ( $\text{I}^-$ ). A schematic of the experimental system is shown in Fig. 1.

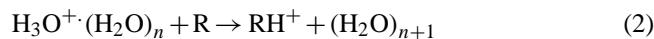
Mixtures initially containing 1.62 M methylglyoxal and 3.1 M  $(\text{NH}_4)_2\text{SO}_4$  or 5.1 M NaCl were prepared using Millipore water as described in the previous section. After the desired reaction time had passed, the mixtures were diluted with Millipore water until the salt concentration was 0.2 M. Reaction time was generally  $>24$  h, which was sufficient time for significant light absorption and surface tension depression to develop in the methylglyoxal/ $(\text{NH}_4)_2\text{SO}_4$  solutions. Reaction kinetics at short times were investigated as follows: a small amount of reaction mixture initially containing 1.62 M methylglyoxal and 3.1 M  $(\text{NH}_4)_2\text{SO}_4$  was diluted 2 min after mixing. Another sample of the same bulk reaction mixture was diluted 38 min after mixing. The mass spectra of these samples were measured using Aerosol-CIMS immediately after dilution.

Two control experiments were performed, the first in which a 0.2 M  $(\text{NH}_4)_2\text{SO}_4$  solution at pH=2 and the second

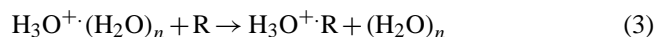
in which a 0.05 M methylglyoxal solution was atomized and analyzed using Aerosol-CIMS. Additional control experiments to test the performance of Aerosol-CIMS in the high mass detection mode were performed using a solution of 0.2 M NaCl and 3.9 mM poly(ethylene glycol) (PEG) (Sigma Aldrich, 570–630 amu) in Millipore water. The instrument was calibrated using aerosol-phase succinic acid ( $C_4H_6O_4$ ). Aerosols were generated by atomizing a solution of 0.001 M succinic acid in Millipore water. Since the liquid water content of the aerosol particles was not known, we assume that the aerosol mass measured by the SMPS was comprised of 100% succinic acid and report the calculated sensitivity and detection limit values as lower and upper limits, respectively. The instrument sensitivity to aerosol-phase succinic acid was measured using the  $I^-$  detection scheme to be  $\geq 100 \text{ Hz ppt}^{-1}$  with a detection limit of  $\leq 0.01 \mu\text{g m}^{-3}$ . Using the  $H_3O^+(H_2O)_n$  scheme, the sensitivity to succinic acid was  $\geq 66 \text{ Hz ppt}^{-1}$  and the detection limit was  $\leq 0.02 \mu\text{g m}^{-3}$ .

The dilute solutions were aerosolized with  $N_2$  using a constant output atomizer (TSI 3076), forming submicron particles. The aerosol stream was combined with a dry  $N_2$  dilution flow, resulting in a relative humidity of 50–60% as measured with a hygrometer (Vaisala). The particle population was characterized using a scanning mobility particle sizer (SMPS) (Grimm Technologies, TSI). The aerosol had a lognormal size distribution with a typical geometric standard deviation of 1.8 and a mean volume-weighted particle radius of  $119 \pm 1 \text{ nm}$ . Typical number concentrations were  $7 \times 10^4 \text{ cm}^{-3}$ . The aerosol stream passed through a 23 cm-long, 1.25 cm ID PTFE tube wrapped in heating tape in order to volatilize the organics before entering the chemical ionization region of the mass spectrometer. The external temperature of the inlet was maintained at  $135^\circ\text{C}$  using a thermocouple and temperature controller (Staco Energy). No increase in signal was observed when the inlet temperature was increased to  $160^\circ\text{C}$ . Some experiments were performed with no inlet heating in order to test for species which were volatile at room temperature.

Flow through the aerosol inlet into the chemical ionization region was maintained at 3 SLPM using a critical orifice. The chemical ionization (CI) region consists of a 3.5 cm ID stainless steel manifold which is 3.8 cm long. Pressure in the CI region is maintained at 45–55 Torr by a mechanical pump (Varian DS302). For the negative ion detection scheme,  $I^-$  reagent ions were generated by flowing dilute  $CH_3I$  (Alfa Aesar, 99.5%) in 3 SLPM  $N_2$  (Tech Air, 99.999%) through a  $^{210}\text{Po}$  ionizer (NRD). The ionizer was mounted perpendicular to the CI region. For detection with  $H_3O^+(H_2O)_n$ , ions were generated by flowing a combined stream of 2 SLPM  $N_2$  bubbled through Millipore water and 3 SLPM dry  $N_2$  through the ionizer. Ion-neutral reaction times were 20–30 ms. For the  $H_3O^+(H_2O)_n$  detection scheme, the predominant peaks in our spectra are  $H_3O^+(H_2O)_2$  at 55 amu and  $H_3O^+(H_2O)_3$  at 73 amu. The reagent ions react with the neutral species through proton transfer (Hearn and Smith, 2004a):



or ligand switching (Blake et al., 2009) :



and the species are then detected as the protonated analyte molecule or its cluster with  $H_2O$ . In the  $I^-$  detection scheme the analyte molecules form clusters with  $I^-$  via a ligand-switching reaction:



or they are ionized via proton abstraction:



Ions passed from the CI region through a 0.05 cm-ID charged orifice into a collisional dissociation chamber (CDC) which was maintained at 5 Torr by a mechanical pump (Varian DS402). Ions may be accelerated through this region using a series of biased cylindrical lenses in order to control clustering. The CDC is separated from the MS prechamber ( $\sim 10^{-4}$  Torr) by a second charged orifice plate (ID=0.05 cm). The prechamber contains an ion optics assembly (Extrel CMS) and is separated by a 0.2 cm-ID orifice from the final chamber ( $\sim 10^{-7}$  Torr) which houses the 19 mm quadrupole and detector (Extrel CMS). The final two chambers are differentially pumped by identical turbomolecular pumps (Varian TV-301 Navigator) backed by a single mechanical pump (Varian DS302). For regular operation the RF operating frequency for the mass spectrometer was 1.2 MHz; for high mass mode a 0.88 MHz RF supply was used (Extrel CMS).

## 2.5 DFT calculations

Geometry optimizations and energy calculations were performed using Jaguar 6.0 (Schrodinger, Inc.) with the ChemBio3D interface (CambridgeSoft) in order to evaluate the UV-Vis absorption of potential products and the energetics of reaction pathways, and to evaluate the interactions of proposed product molecules with  $I^-$  for CIMS detection. Density functional theory (DFT) with the B3LYP functional and the cc-pVTZ(-f) basis set (Kendall et al., 1992) was used to predict the HOMO-LUMO energy difference (and thus UV-Vis absorption wavelengths) of proposed products. For purposes of comparison with Krizner et al. (2009) some additional calculations were performed with the 6-311G\*\* basis set and Poisson-Boltzmann solvation (water solvent,  $\epsilon=80.37$ , probe radius =  $1.40 \text{ \AA}$ ). The Gibbs free energy of solvated species was calculated using half the gas phase entropy following Krizner et al. (2009).

For the CIMS ion-molecule reaction calculations, DFT was used with the B3LYP functional and the ERMLER2 basis set, which allows the treatment of iodine via the use of effective core potentials (Lajohn et al., 1987). The free energy

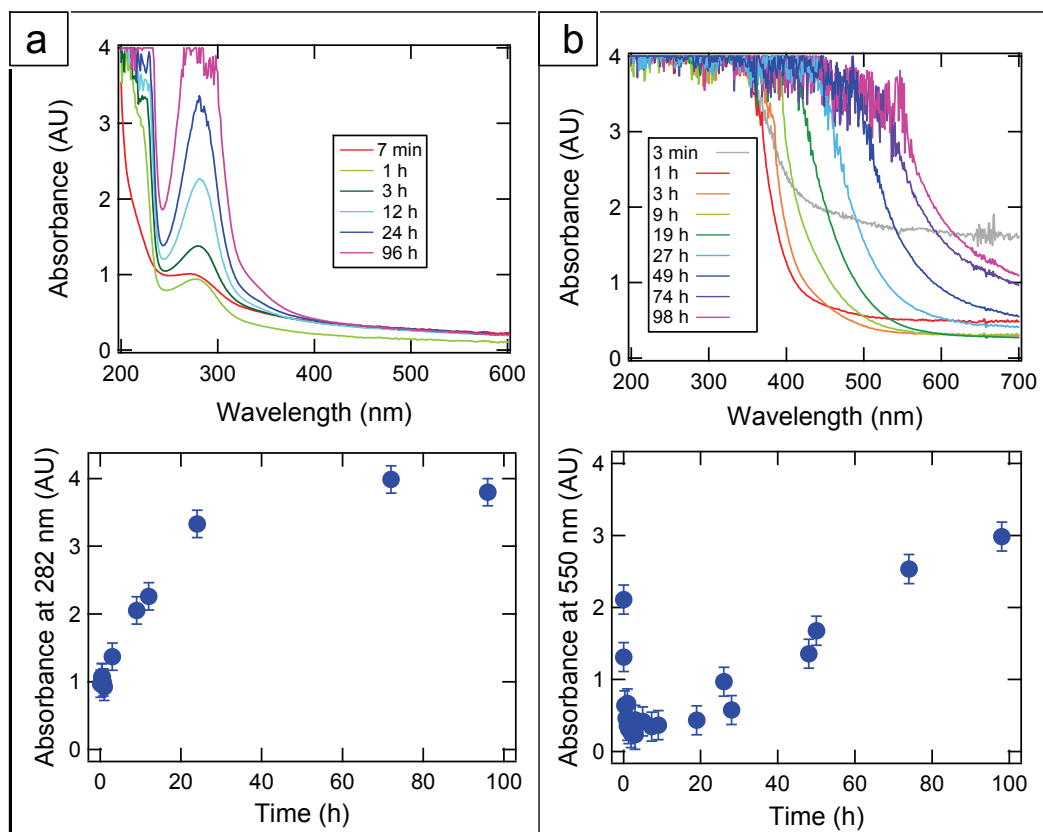


**Fig. 2.** UV-Vis spectra of aqueous solutions containing 3.1 M (NH<sub>4</sub>)<sub>2</sub>SO<sub>4</sub> and (a) 16.2 mM methylglyoxal and (b) 1.62 M methylglyoxal as a function of time after mixing. Absorbance is shown as a function of wavelength in the upper panels, and absorbance at selected wavelengths is shown in the lower panels. Error bars reflect uncertainty in the measured absorbances based on variation observed in the baseline signal.

change for the ligand-switching reaction or proton abstraction was calculated. For the ligand switching reactions several geometries for the cluster of the analyte molecule with I<sup>-</sup> were tested for each species, and in some cases several stable cluster geometries (local minima) were found. In each case,  $\Delta G$  for the lowest-energy cluster geometry (global minimum) is reported. The free energy values reported here are from the output of the 298.15 K vibrational frequency calculation and no further corrections were applied.

### 3 Results and discussion

Solutions containing  $\geq 0.16$  M methylglyoxal and (NH<sub>4</sub>)<sub>2</sub>SO<sub>4</sub> became visibly colored immediately after mixing and became progressively darker in color with time. The color varied noticeably with initial methylglyoxal concentration; solutions with higher initial concentrations of methylglyoxal were darker in color.

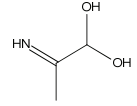
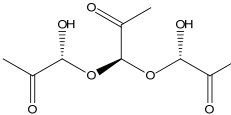
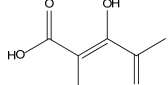
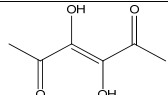
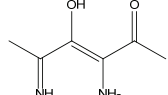
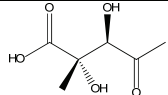
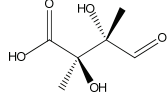
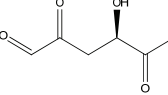
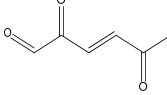
#### 3.1 UV-Vis absorption

The products formed by methylglyoxal in aqueous solutions containing (NH<sub>4</sub>)<sub>2</sub>SO<sub>4</sub> or NH<sub>4</sub>NO<sub>3</sub> absorb light at UV and visible wavelengths (ref. Figs. 2–3 and Supplementary Information: <http://www.atmos-chem-phys.net/10/997/2010/acp-10-997-2010-supplement.pdf>).

##### 3.1.1 Experimental results

Aqueous methylglyoxal solutions with no salt have a broad absorbance peak at 290 nm at ambient temperatures (Nemet et al., 2004). A kinetics study of 16.2 mM methylglyoxal in 3.1 M (NH<sub>4</sub>)<sub>2</sub>SO<sub>4</sub> (aq) (Fig. 2a) shows that after a delay of  $\sim 1$  h, peaks grow in at 213 nm and 282 nm with roughly exponential time dependence. The measured absorbance of a solution of 1.62 M aqueous methylglyoxal and 3.1 M (NH<sub>4</sub>)<sub>2</sub>SO<sub>4</sub> initially increases upon mixing across all wavelengths (Fig. 2b). This initial increase in baseline absorption could indicate either formation of at least one light-absorbing reaction intermediate that is consumed in later steps of the mechanism, or a transient change in the bulk properties (e.g. refractive index, density) of the solutions. After 1 h, the

**Table 1.** Proposed reaction products. Predictions for the energy of the gas phase HOMO-LUMO transition and the wavelength of UV-Vis absorption from DFT B3LYP/cc-pvtz(-f) simulations are shown. References are indicated by: 1) Nemet et al. (2004), 2) Zhao et al. (2006), 3) Krizner et al. (2009).

	Molecule	Ref.	energy (eV)	$\lambda$ (nm)
a)		This work	6.757	183.5
b)		1,2	5.728	216.5
c)		This work	4.574	271.1
d)		This work	3.536	350.6
e)		This work	3.354	369.6
f)		This work	6.247	198.5
g)		This work	5.751	215.6
h)		3	3.872	320.2
i)		3	3.661	338.7

absorption spectrum is saturated for  $\lambda \leq 360$  nm, and the baseline at high wavelengths returns to  $<0.5$  AU. With increasing time, the saturated region of the spectrum extends to longer wavelengths and the tail shows increasing absorption at high wavelengths ( $\lambda > 500$ ). Significant absorption at 550 nm is exhibited at  $<1$  h and after 12 h, with absorption at up to 700 nm developing within 2–3 days.

The effect of initial methylglyoxal concentration on the UV-Vis spectra of solutions containing 3.1 M  $(\text{NH}_4)_2\text{SO}_4$  24 h after mixing is shown in Fig. 3a. The absorbance at 282 nm after 3.0 h is linearly dependent on the initial methylglyoxal concentration. The effect of pH on the production of light-absorbing products in solutions initially containing 1.62 mM methylglyoxal and 3.1 M  $(\text{NH}_4)_2\text{SO}_4$  is shown in

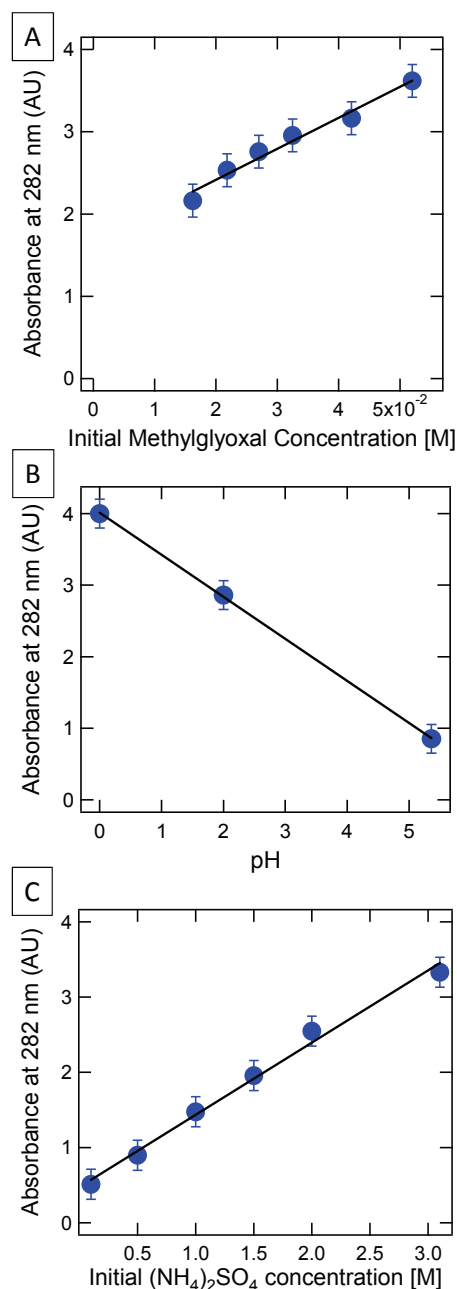


**Fig. 3.** Absorbance at 282 nm of aqueous solutions containing (a) 3.1 M  $(\text{NH}_4)_2\text{SO}_4$  and varying initial concentrations of methylglyoxal, pH=2.0( $\pm 0.1$ ), 3.0 h after mixing. (b) 3.1 M  $(\text{NH}_4)_2\text{SO}_4$ , 1.62 mM methylglyoxal, and varying pH 24 h after mixing, and (c) 16.2 mM methylglyoxal and varying initial concentrations of  $(\text{NH}_4)_2\text{SO}_4$ , 24 h after mixing. Error bars reflect uncertainty in the measured absorbances based on variation observed in the baseline signal.

Fig. 3b. The absorbance at 282 nm of solutions initially containing 16.2 mM methylglyoxal 24 h after mixing is linearly dependent on the initial  $(\text{NH}_4)_2\text{SO}_4$  concentration, as shown in Fig. 3c.

Control samples containing 1.62 M methylglyoxal and 5.1 M NaCl or 1.18 M Na<sub>2</sub>SO<sub>4</sub> exhibited UV-Vis spectra similar to aqueous methylglyoxal in the absence of salt after 24 h. A sample initially containing 1.62 M methylglyoxal and 3.1 M (NH<sub>4</sub>)<sub>2</sub>SO<sub>4</sub> was protected from light until analysis by covering the reaction vessel with aluminum foil, and the resulting spectrum at 24 h was identical to that of an unprotected solution with the same composition. This indicates that the reactions leading to light-absorbing compounds in this study are not photochemical. The results of these control experiments can be found in the Supplementary Material (<http://www.atmos-chem-phys.net/10/997/2010/acp-10-997-2010-supplement.pdf>).

### 3.1.2 DFT calculations

The results of our B3LYP/cc-pVTZ(-f) calculations of the HOMO-LUMO energy difference (and thus UV-Vis absorption wavelengths) of several proposed products are listed in Table 1. When molecules absorb light, their electrons may be promoted from the HOMO (highest occupied molecular orbital) to the LUMO (lowest unoccupied molecular orbital). The energy difference between these levels corresponds to the wavelength of absorption according to  $E=hc/\lambda$  where  $E$  is the HOMO-LUMO energy difference,  $h$  is Planck's constant,  $c$  is the speed of light in vacuum, and  $\lambda$  is the wavelength.

Our calculations were made for gas-phase molecules. Meller et al. (1991) reported that gas-phase methylglyoxal has an absorption peak at 280 nm. Our B3LYP/cc-pVTZ(-f) calculations predict that gas-phase, unhydrated methylglyoxal has an absorption peak at 291.1 nm. Therefore we estimate that our predictions for these molecules in the absence of solvent effects are accurate to within  $\sim 12$  nm. Further deviation between the theoretical results and experiment may result from solvent effects. The  $n$  to  $\pi^*$  excitation band characteristic of carbonyl compounds appears at  $\sim 290$  nm and is known to shift toward lower wavelengths (blue shift) for a molecule in aqueous solvent compared to the gas phase (Skoog et al., 1997). For acetone this shift is approximately 12 nm, and for crotonaldehyde the shift is  $\sim 30$  nm (Bayliss and McRae, 1954). Therefore, we can estimate an error range of ( $-12$  nm,  $+42$  nm) for the predicted absorbances. Note that aqueous methylglyoxal solutions will contain a mixture of mono- and di-hydrated methylglyoxal, aldol condensation products, and hemiacetal oligomers (Krizner et al., 2009), so it is less straightforward to map the observed spectrum of aqueous methylglyoxal to the gas-phase absorbance of a single molecule for purposes of this discussion.

Referring to Scheme 1, Krizner et al. (2009) showed that aldol pathway (2) is thermodynamically favorable for aqueous methylglyoxal (they did not study pathway (1)). Our B3LYP/6-311G\*\* calculations with Poisson-Boltzmann solvation show that  $\Delta G=10.5$  kcal mol<sup>-1</sup> for the formation of the pathway (1) enol from singly hydrated methylglyoxal,

close to Krizner et al.'s value of 11.9 kcal mol<sup>-1</sup> for the formation of the pathway (2) enol, suggesting that both enol species should be present in small quantities at equilibrium. Aldol addition via pathway (1) is likely to terminate after dimer or trimer formation due to the formation of organic acid or ketone end groups (e.g. species (c–g), Table 1). It is not energetically favorable for aldol addition at ketone end groups to continue via pathway (1) due to steric hindrance from the methyl group. Instead, these ketones may form an enol and follow pathway (2) for continuing aldol addition. Additionally, because of the methyl group, many of the products of aldol addition via pathway (1) cannot proceed with dehydration (e.g. species (g), Table 1). Pathway (2) results in carbonyl termination (e.g. species (h) and (i), Table 1) and therefore aldol condensation could propagate beyond the trimer.

Referring to Fig. 2a, based on our B3LYP/cc-pvtz(-f) predictions, the species absorbing at 213 nm could correspond to an aldol addition product such as species (f) or (g) in Table 1. Acetals such as species (b) in Table 1 may also absorb at this wavelength. As described above, we estimate the error range of our theoretically predicted absorbances compared to the observed aqueous-phase spectra to be roughly ( $-12$  nm,  $+42$  nm). Therefore the absorbance band at 286 nm could correspond to a species predicted to absorb within the range  $274$  nm  $< \lambda < 328$  nm. Species which lie within this range include the pathway (2) aldol addition product species (h), which is predicted to absorb at 320 nm. Given the approximate nature of these lower and upper bounds, another candidate species could be species (c) which is predicted to absorb at 271.1 nm. Species (c) is the aldol condensation product corresponding to the aldol addition product (f). C=N bonds could also contribute to the observed absorbance.

### 3.2 Surface tension

Solutions containing 3.1 M (NH<sub>4</sub>)<sub>2</sub>SO<sub>4</sub> and varying initial concentrations of methylglyoxal exhibit significant surface tension depression compared to 3.1 M (NH<sub>4</sub>)<sub>2</sub>SO<sub>4</sub> solutions without organics (ref. Fig. 4). The surface tension depression follows a Langmuir-like dependence on initial methylglyoxal concentration, with a minimum (saturation) surface tension,  $\sigma_{\min}$ , of  $41 (\pm 2)$  dynes cm<sup>-1</sup> based on a fit to the data using the following equation:

$$\sigma = \sigma_0 - S \frac{bM_0}{1 + bM_0} \quad (6)$$

where  $\sigma$  is the surface tension,  $\sigma_0$  is the surface tension of the solution with no methylglyoxal,  $M_0$  is the initial methylglyoxal concentration, and  $S$  and  $b$  are fit parameters. Values of  $\sigma_0$  for (NH<sub>4</sub>)<sub>2</sub>SO<sub>4</sub> (aq) and NaCl (aq) were taken from the International Critical Tables (2003). The physical interpretation of  $S$  is the surface tension depression when the surface is saturated, such that  $\sigma_{\min} = \sigma_0 - S$ , and  $b$  is an equilibrium coefficient that describes surface-bulk partitioning. A

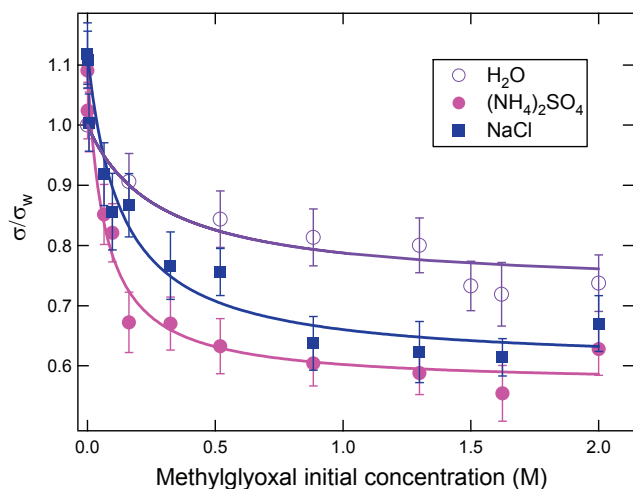


**Fig. 4.** Results of pendant drop tensiometry measurements of aqueous mixtures as a function of initial methylglyoxal concentration for aqueous solution, 3.1 M (NH<sub>4</sub>)<sub>2</sub>SO<sub>4</sub> (aq), and 5.1 M NaCl (aq). The ratio of measured surface tension to the measured surface tension of Millipore water is shown. The measurements were made  $\geq 24$  h after mixing. Each point reflects the weighted average of five to eight measurements, and the error bars represent the standard deviation in the raw data. The best fit curve to each data set based on Eq. (6) is also shown.

time series was performed on a solution initially containing 1.62 M methylglyoxal and 3.1 M (NH<sub>4</sub>)<sub>2</sub>SO<sub>4</sub>. The measured surface tension fluctuated for 2.5 h before stabilizing at 45 ( $\pm 1$ ) dynes cm<sup>-1</sup>, then slowly decreased over the next 21.5 h to the minimum value (41 ( $\pm 2$ ) dynes cm<sup>-1</sup>). Control experiments were performed in order to evaluate the role of (NH<sub>4</sub>)<sub>2</sub>SO<sub>4</sub>. For aqueous methylglyoxal solutions with no salts present  $\sigma_{\min} = 52$  ( $\pm 3$ ) dynes cm<sup>-1</sup>. Therefore, while hydrated methylglyoxal and/or the oligomers it forms in aqueous solution are surface-active, the overall surface-tension lowering effect is less than when (NH<sub>4</sub>)<sub>2</sub>SO<sub>4</sub> is present in solution. Solutions containing 5.1 M NaCl and varying amounts of methylglyoxal follow a trend similar to that of the (NH<sub>4</sub>)<sub>2</sub>SO<sub>4</sub> solutions, with  $\sigma_{\min} = 43$  ( $\pm 2$ ) dynes cm<sup>-1</sup> (Fig. 4).

Surface tension depression for methylglyoxal solutions containing 5.1 M NaCl or 3.1 M (NH<sub>4</sub>)<sub>2</sub>SO<sub>4</sub> is greater than that observed for aqueous methylglyoxal in the absence of salts. The observed enhancement in surface tension depression is likely to be a physical effect of the salts rather than an effect of especially surface-active products formed by a chemical reaction of methylglyoxal with the salts. High salt concentrations can result in a decreased critical micelle concentration due to charge screening, and thus cause enhanced film formation (Matijevic and Pethica, 1958; Li et al., 1998). Salts can also decrease the solubility of organics, commonly referred to as “salting out” (Setschenow, 1889), possibly resulting in surface film formation. Salts have commonly been

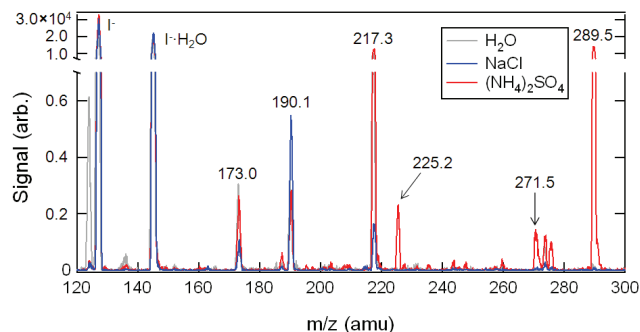


**Fig. 5.** Negative-ion mass spectrum of aerosolized aqueous solutions initially containing methylglyoxal alone (grey) or with NaCl (blue) or (NH<sub>4</sub>)<sub>2</sub>SO<sub>4</sub> (red) (see text for details). Select product species were detected using I<sup>-</sup> as the reagent ion. Peaks associated with I<sup>-</sup> and its cluster with H<sub>2</sub>O as well as the mass-to-charge ratios of product peaks are labeled.

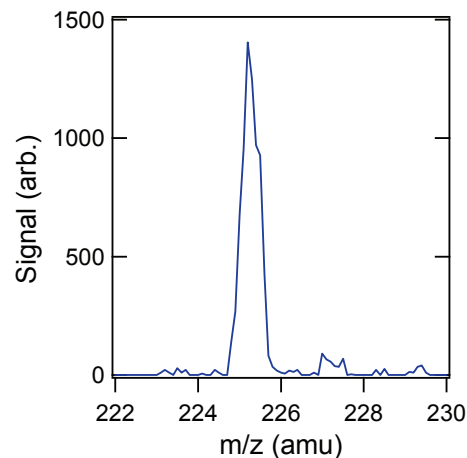


**Fig. 6.** Detail of a 0.5 amu-resolution negative ion mass spectrum of aerosolized methylglyoxal/(NH<sub>4</sub>)<sub>2</sub>SO<sub>4</sub> solution. A peak at 225.2 amu and a satellite peak at 227.2 amu are shown.

observed to enhance the surface tension lowering effects of HULIS and organic diacids (Shulman et al., 1996; Kiss et al., 2005; Asa-Awuku et al., 2008).

Glyoxal was previously observed not to be surface-active in hydrated form or to form surface-active products in aqueous (NH<sub>4</sub>)<sub>2</sub>SO<sub>4</sub> solutions (Shapiro et al., 2009). Compared with glyoxal, the methyl group adds hydrophobicity to methylglyoxal and its oligomer products, increasing their surface activity.

### 3.3 Aerosol-CIMS

Representative Aerosol-CIMS mass spectra for the aqueous methylglyoxal, methylglyoxal/NaCl and methylglyoxal/(NH<sub>4</sub>)<sub>2</sub>SO<sub>4</sub> systems using I<sup>-</sup> or H<sub>3</sub>O<sup>+</sup>(H<sub>2</sub>O)<sub>*n*</sub> as the reagent ion are shown in Figs. 5–8. The spectra represented in these figures have mass



resolution of 1 amu except as noted; peak assignments were made using 0.5 amu resolution spectra.

### 3.3.1 Negative ion detection with $I^-$

A summary of proposed peak assignments for the mass spectra in Fig. 5 using  $I^-$  as the reagent ion can be found in Table 2. Significant signal in the aqueous methylglyoxal control spectrum is observed at 173.0, 190.1, 217.3, and 273.5 amu. Most of the peaks in the methylglyoxal/ $(NH_4)_2SO_4$  mass spectrum are also found in the methylglyoxal/NaCl spectrum. Increased signal appears at 271.5, 273.5, and 289.5 amu in the methylglyoxal/ $(NH_4)_2SO_4$  spectrum. Peaks unique to methylglyoxal/ $(NH_4)_2SO_4$  include 225.2 and 275.6 amu. The peak at 217.3 amu is consistent with the cluster of  $I^-$  with singly hydrated methylglyoxal. The presence of multiple peaks  $>217.3$  amu is indicative of dimer formation.

#### DFT calculations

$I^-$  has previously been used as a reagent ion with Aerosol-CIMS to detect organic acids in aerosols (McNeill et al., 2007, 2008). Since the product species expected to be present in this reactive system (methylglyoxal, acetal/hemiacetal oligomers, aldol condensation oligomers) have not been previously detected via the  $I^-$  ionization scheme, we performed ab initio calculations in order to characterize the interaction of proposed product species with  $I^-$ . The results are summarized in Table 3. Optimized geometries and calculated energies for each species can be found in the Supplementary Material (<http://www.atmos-chem-phys.net/10/997/2010/acp-10-997-2010-supplement.pdf>). Our calculations show that the formation of clusters between  $I^-$  and several of the acetal and hemiacetal species proposed by Zhao et al. (2006) via ligand switching with  $I^- \cdot H_2O$  is thermodynamically favorable, particularly when two or more hydroxyl moieties are available to interact with  $I^-$  simultaneously. This is also the case for hydrated methylglyoxal species. Non-hydrated methylglyoxal is not predicted to form strong clusters with or be ionized by  $I^-$ , and therefore we do not expect to detect it using this approach. Aldol addition products from either pathway (e.g. species (d) or (h) from Table 3), if present, should be detected as their clusters with  $I^-$ . The only aldol condensation products which we predict to form strong clusters with  $I^-$  are those species which terminate in a carboxylic acid group (e.g. species (f) from Table 3). We do not expect to observe products of aldol pathway (2) (ref. Scheme 1) such as species (c) from Table 3 with this ionization scheme.

#### Volatile species

The peaks at 173.0, 190.1, and 217.3 amu were present in the same magnitude whether the volatilization inlet heat was turned on or off, indicating that these signals are associated

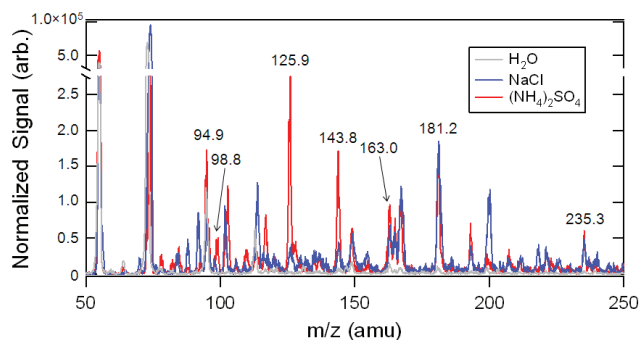


**Fig. 7.** Positive ion mass spectrum of aerosolized aqueous solutions initially containing methylglyoxal alone (grey) or with NaCl (blue) or  $(NH_4)_2SO_4$  (red).  $H_3O^+ \cdot (H_2O)_n$  was the chemical ionization reagent. The mass-to-charge ratios of select product peaks are labeled.

with volatile species. The signal observed at 173.0 amu is consistent with formic acid ( $I^- \cdot HCOOH$ ). Gas-phase formic acid has been previously observed to be an oxidation product of organic acids in aerosols; it was detected at this mass using Aerosol-CIMS with the same ionization scheme used here (McNeill et al., 2008). The signal we observe at 190.1 amu is consistent with a molecular formula of  $I^- \cdot CH_5O_2N$ , but it is more likely due to the water cluster of the formic acid peak.

#### (Hemi)acetals and aldol condensation products

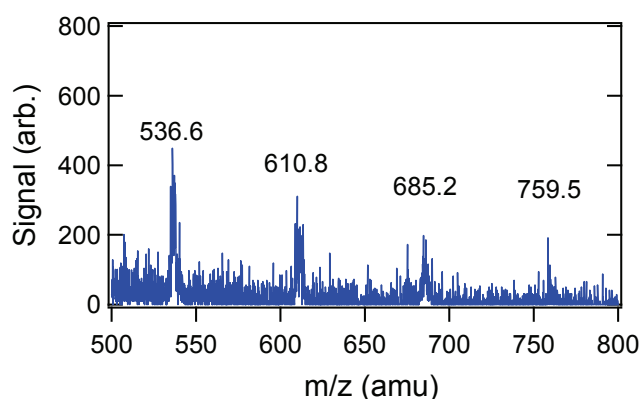
The peak at 271.5 amu is attributed to the molecular formula  $I^- \cdot C_6H_8O_4$ , which could correspond to the pathway (1) aldol condensation dimers or pathway (2) aldol addition products (ref. Scheme 1 and Table 2). 289.5 amu is consistent with  $I^- \cdot C_6H_{10}O_5$ , and therefore can be matched to acetal and hemiacetal dimers proposed by others (Nemet et al., 2004; Loeffler et al., 2006; Zhao et al., 2006) or pathway (1) aldol addition products. Small amounts of signal at both of these masses are present in the methylglyoxal/NaCl spectrum, and temperature control experiments indicate that these species are semivolatile.

Since succinic acid, an organic diacid, is expected to cluster strongly with  $I^-$  we may assume that the instrument sensitivity to succinic acid ( $100 \text{ Hz ppt}^{-1}$ ) is an upper limit for the sensitivity to these species. Using this assumption, we estimate lower bounds for the production rates of the species at 271.5 and 289.5 to be  $\geq 10^{-3} \text{ M min}^{-1}$  and  $\geq 10^{-2} \text{ M min}^{-1}$ , respectively.

The peaks at 273.5 and 275.6 amu are assigned the molecular formulas  $I^- \cdot C_6H_{10}O_4$  and  $I^- \cdot C_6H_{12}O_4$ , respectively. These molecular formulas, since they each contain six carbons, are consistent with the addition of two methylglyoxal monomers. Possible structures are shown in Table 2, but the formation mechanisms of these species in the methylglyoxal/ $(NH_4)_2SO_4$  system are not known.

**Table 2.** Proposed peak assignments for Aerosol-CIMS mass spectra with  $\text{I}^-$  as the reagent ion. See text for details.

$m/z$ (amu) $\pm 0.5$ amu	Ion formula	Molecular formula	Possible Structure(s)
217.3	$\text{I}^- \text{C}_3\text{H}_6\text{O}_3$	$\text{C}_3\text{H}_6\text{O}_3$	
225.2	$\text{C}_6\text{H}_9\text{O}_7\text{S}^-$	$\text{C}_6\text{H}_{10}\text{O}_7\text{S}$	
271.5	$\text{I}^- \text{C}_6\text{H}_8\text{O}_4$	$\text{C}_6\text{H}_8\text{O}_4$	
273.5	$\text{I}^- \text{C}_6\text{H}_{10}\text{O}_4$	$\text{C}_6\text{H}_{10}\text{O}_4$	
275.6	$\text{I}^- \text{C}_6\text{H}_{12}\text{O}_4$	$\text{C}_6\text{H}_{12}\text{O}_4$	
289.5	$\text{I}^- \text{C}_6\text{H}_{10}\text{O}_5$	$\text{C}_6\text{H}_{10}\text{O}_5$	

**Fig. 8.** Detail of a positive ion mass spectrum of an aerosolized methylglyoxal/ $(\text{NH}_4)_2\text{SO}_4$  solution. Spectrum was taken in high-mass mode with  $\text{H}_3\text{O}^+(\text{H}_2\text{O})_n$  as the reagent ion.

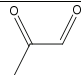
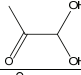
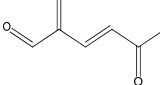
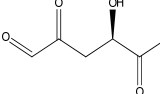
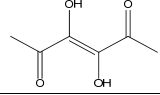
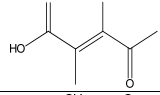
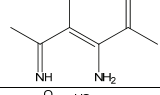
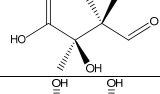
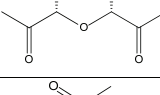
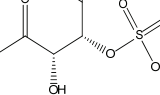
### Sulfur-containing species

The peak at 225.2 amu features a satellite peak at 227.2 amu with an abundance roughly consistent with the expected 95:4

ratio of the stable isotopes of sulfur  $^{32}\text{S}$  and  $^{34}\text{S}$  (Fig. 6), suggesting a compound containing sulfur. Either a molecule with a molecular weight of 226.2 amu (in the case of proton abstraction) or 98.3 amu (in the case of a cluster with  $\text{I}^-$ ) would be consistent with the 225.2 amu mass-to-charge ratio. The species with  $m/z$  225.2 amu was observed to be non-volatile at room temperature. One possible molecular formula for this species is  $\text{C}_6\text{H}_9\text{O}_7\text{S}^-$ . The proposed structure for the  $\text{C}_6\text{H}_9\text{O}_7\text{S}^-$  organosulfate species is shown in Table 1. Our DFT calculations predict that proton abstraction from the sulfate group by  $\text{I}^-$ , rather than clustering via the ligand-switching reaction, is thermodynamically favorable for this species. Kinetics studies show that the signal at 225.2 amu develops within approximately 30 min of mixing. Assuming an upper limit sensitivity of  $100 \text{ Hz ppt}^{-1}$  for this species we can estimate a production rate of  $\geq 4 \times 10^{-3} \text{ M min}^{-1}$ .

$\text{H}_2\text{SO}_4$  may cluster with  $\text{I}^-$  or undergo proton abstraction.  $\text{I}^- \cdot \text{H}_2\text{SO}_4$ , if present, would also appear at 225.2 amu and display a satellite peak at 227.2 amu. In order to test for this

**Table 3.** Proposed reaction products. Predictions for the free energy change of the ligand switching reaction with  $\text{I}^- \cdot \text{H}_2\text{O}$  to form a cluster with  $\text{I}^-$  based on DFT B3LYP/ERMLER2 calculations are shown. Strong clustering is indicated in bold.

Molecule	Molecular formula	Molecular weight (amu)	DFT $\Delta G$ ( $\text{kJ mol}^{-1}$ ) $\text{R} + \text{I}^- \cdot \text{H}_2\text{O} \rightarrow \text{I}^- \cdot \text{R} + \text{H}_2\text{O}$
a) 	$\text{C}_3\text{H}_4\text{O}_2$	72.1	-3.14
b) 	$\text{C}_3\text{H}_6\text{O}_3$	90.1	<b>-44.1</b>
c) 	$\text{C}_6\text{H}_6\text{O}_3$	126.1	-16.1
d) 	$\text{C}_6\text{H}_8\text{O}_4$	144.1	<b>-34.3</b>
e) 	$\text{C}_6\text{H}_8\text{O}_4$	144.1	-1.07
f) 	$\text{C}_6\text{H}_8\text{O}_4$	144.1	<b>-49.2</b>
g) 	$\text{C}_6\text{H}_{10}\text{O}_2\text{N}_2$	141.2	-7.77
h) 	$\text{C}_6\text{H}_{10}\text{O}_5$	162.1	<b>-65.2</b>
i) 	$\text{C}_6\text{H}_{10}\text{O}_5$	162.1	<b>-65.7</b>
j) 	$\text{C}_6\text{H}_{10}\text{O}_7\text{S}$	226.2	H-abstraction from the sulfate group: <b>-118.0</b>

possibility a control experiment was performed in which a 0.2 M  $(\text{NH}_4)_2\text{SO}_4$  solution at pH=2 (similar to the conditions of the solutions with methylglyoxal) was atomized and analyzed using Aerosol-CIMS. There was no peak at 225.2 amu in the spectrum of the control, suggesting that the observed peak in the methylglyoxal/ $(\text{NH}_4)_2\text{SO}_4$  spectrum cannot be attributed to inorganic sulfate or sulfuric acid. Hearn and Smith (2006b) previously used Aerosol-CIMS with  $\text{SF}_6^-$  as the parent ion and a volatilization temperature of 220 °C to detect aerosol sulfate (as  $\text{HSO}_4^-$ , 97 amu). We observed a small ( $\sim 300$  cps) peak at 97 amu in the methylglyoxal/ $(\text{NH}_4)_2\text{SO}_4$  spectra but not in the control experiment. We note that organosulfates have previously been observed to decompose during negative ion mass spectrometry to generate  $\text{HSO}_4^-$  (Attygalle et al., 2001).

### 3.3.2 Positive ion detection using $\text{H}_3\text{O}^+(\text{H}_2\text{O})_n$

$\text{H}_3\text{O}^+(\text{H}_2\text{O})_n$  is commonly used to detect VOCs, including methylglyoxal (Zhao et al., 2006; Blake et al., 2009) and has been used to detect volatilized aerosol organics including levoglucosan from tobacco and wood smoke, limonene SOA (Hearn and Smith, 2004a) and pyridine (Thornberry et al., 2009). Table 4 lists the proposed peak assignments for the spectra in Fig. 7 which were obtained using  $\text{H}_3\text{O}^+(\text{H}_2\text{O})_n$  as the reagent ion. More peaks appear in these spectra than in those obtained using  $\text{I}^-$  as a reagent ion because proton transfer via  $\text{H}_3\text{O}^+(\text{H}_2\text{O})_n$  is favorable for a wider variety of organics than ligand switching or proton abstraction via  $\text{I}^-$  is. The aqueous methylglyoxal control spectrum features peaks at 94.9 amu and 112.9 amu. Signal at

**Table 4.** Proposed peak assignments for Aerosol-CIMS mass spectra with  $\text{H}_3\text{O}^+(\text{H}_2\text{O})_n$  as the reagent ion. See text for details.

$m/z$ (amu) $\pm 0.5$ amu	Ion formula	Molecular formula	Possible Structure(s)
125.9	$\text{C}_6\text{H}_6\text{O}_2\text{N}^+$	$\text{C}_6\text{H}_7\text{O}_2\text{N}$	
143.8	$\text{C}_6\text{H}_{10}\text{O}_3\text{N}^+$ $\text{C}_6\text{H}_8\text{O}_2\text{N}^+\text{H}_2\text{O}$	$\text{C}_6\text{H}_9\text{O}_3\text{N}$ $\text{C}_6\text{H}_7\text{O}_2\text{N}$	
163.0	$\text{C}_6\text{H}_{11}\text{O}_5^+$	$\text{C}_6\text{H}_{10}\text{O}_5$	
	$\text{C}_6\text{H}_9\text{O}_4^+\text{H}_2\text{O}$	$\text{C}_6\text{H}_8\text{O}_4$	
165.0	$\text{C}_6\text{H}_{13}\text{O}_5^+$	$\text{C}_6\text{H}_{12}\text{O}_5$	
	$\text{C}_6\text{H}_{11}\text{O}_4^+\text{H}_2\text{O}$	$\text{C}_6\text{H}_{10}\text{O}_4$	
167.1	$\text{C}_6\text{H}_{15}\text{O}_5^+$	$\text{C}_6\text{H}_{14}\text{O}_5$	
	$\text{C}_6\text{H}_{13}\text{O}_4^+\text{H}_2\text{O}$	$\text{C}_6\text{H}_{12}\text{O}_4$	
181.2	$\text{C}_6\text{H}_{13}\text{O}_6^+$ $\text{C}_6\text{H}_{11}\text{O}_5^+\text{H}_2\text{O}$	$\text{C}_6\text{H}_{12}\text{O}_6$ $\text{C}_6\text{H}_{10}\text{O}_5$	
235.3	$\text{C}_9\text{H}_{15}\text{O}_7^+$	$\text{C}_9\text{H}_{14}\text{O}_7$	

94.9, 98.8, 125.9, 143.8, and 163.0 is significantly higher in the methylglyoxal/ $(\text{NH}_4)_2\text{SO}_4$  spectrum as compared to methylglyoxal/ $\text{NaCl}$  or aqueous methylglyoxal. Other notable peaks include 165.0, 167.1, 181.2, and 235.3 amu. The peaks at  $m/z \leq 167.1$  amu (except for 98.8 amu) were

present in the mass spectrum when the volatilization inlet was not heated, indicating that these signals are associated with volatile or semivolatile species.

Methylglyoxal has been detected previously using proton transfer mass spectrometry (Zhao et al., 2006). In

our experiment, the expected  $m/z$  for methylglyoxal coincided with that of one of the parent ions,  $\text{H}_3\text{O}^+(\text{H}_2\text{O})_3$ , at 73.1 amu. Water clusters of methylglyoxal or the hydrated forms would correspond with  $\text{H}_3\text{O}^+(\text{H}_2\text{O})_4$  and  $\text{H}_3\text{O}^+(\text{H}_2\text{O})_5$  at 91.1 and 109.0 amu, respectively. A small signal is observed at 109.0 amu.

The peak at 94.9 amu is consistent with a molecular formula of  $\text{C}_2\text{H}_7\text{O}_4^+$ . This is likely a decomposition product or fragment of a larger compound.

#### *(Hemi)acetals and aldol condensation products*

The peak at 125.9 amu is consistent with the molecular formula  $\text{C}_6\text{H}_8\text{O}_2\text{N}^+$ , corresponding to a type 2 aldol condensation product with a single imine substitution. The peak at 143.8 amu is consistent with a water cluster or aldol addition precursor of that species, or else a type 1 aldol condensation product with one amine or imine substitution. No peaks corresponding to these products were observed using the  $\text{I}^-$  detection scheme. As stated previously, our ab initio calculations showed that products of aldol pathway (2) would not likely be detected using  $\text{I}^-$ . Small amounts of signal at 125.9 amu and 143.8 amu are observed in the methylglyoxal/NaCl spectrum; since N-substitution would not be possible in the methylglyoxal/NaCl system, we will therefore consider this identification of C-N species to be tentative.

The peak at 163.0 amu corresponds to  $\text{C}_6\text{H}_{11}\text{O}_5^+$ ; the species which appear at 289.5 amu in the  $\text{I}^-$  spectrum should appear at this mass. Alternatively, it could be the water cluster of  $\text{C}_6\text{H}_9\text{O}_4^+$ , the type 1 aldol condensation or type 2 aldol addition products which were observed at 271.5 amu in the  $\text{I}^-$  spectrum. Acetal and hemiacetal species also appear at 181.2 and 235.3 amu (see Table 4).

The peaks at 165.0 and 167.1 amu correspond to  $\text{C}_6\text{H}_{13}\text{O}_5^+$  and  $\text{C}_6\text{H}_{15}\text{O}_5^+$ , respectively, or the water clusters of  $\text{C}_6\text{H}_{11}\text{O}_4^+$  and  $\text{C}_6\text{H}_{13}\text{O}_4^+$ . These molecular formulas are consistent with methylglyoxal dimers but the structure and formation mechanism are not known for these species.

#### *Sulfur-containing products*

No peak at 227 amu, which would correspond to  $\text{C}_6\text{H}_{11}\text{O}_7\text{S}^+$ , was observed in the methylglyoxal/ $(\text{NH}_4)_2\text{SO}_4$  spectrum as detected using  $\text{H}_3\text{O}^+(\text{H}_2\text{O})_n$ . To our knowledge organosulfates have not been previously detected using proton transfer ionization.

A peak was observed at 98.8 amu, but no satellite peak was present at 100.8 amu. The signal did not appear in the methylglyoxal/NaCl spectrum. Control experiments confirmed that no peak appeared at 98.8 amu when acidified  $(\text{NH}_4)_2\text{SO}_4$  without methylglyoxal was present in the atomizer solution. Proton transfer ionization is not expected to allow detection of inorganic sulfate or sulfuric acid at this mass. Molecular formulas consistent with this mass-to-charge ratio include  $\text{C}_6\text{H}_{11}\text{O}^+$ ,  $\text{C}_5\text{H}_7\text{O}_2^+$ , or  $\text{C}_4\text{H}_3\text{O}_3^+$ .

#### *High-molecular-weight species*

In order to test our ability to detect high-molecular-weight organics with the Aerosol-CIMS technique, we analyzed aerosols containing NaCl and PEG (570–630 amu) in high-mass mode. We observed two sets of peaks separated by  $44(\pm 1)$  amu (one ethylene oxide unit): {475.8, 518.9, 563.7, 607.4, and 651.5} and {502.4, 546.6, 590.9, 635.1}. This is consistent with the observations of Bogan et al. (2007).

For methylglyoxal/ $(\text{NH}_4)_2\text{SO}_4$  we observed peaks from 536.6–759.5 amu in high-mass mode using  $\text{H}_3\text{O}^+(\text{H}_2\text{O})_n$  as the reagent ion (see Fig. 8). The peaks were separated by 74 amu, which could correspond to a unit of  $\text{C}_3\text{H}_6\text{O}_2$ . We did not observe non-background signal for  $m/z > 300$  amu when using  $\text{I}^-$  as the reagent ion. We previously observed that glyoxal forms oligomers of 500–600 amu in aqueous solution when ammonium sulfate is present (Shapiro et al., 2009). Kalberer et al. (2004) observed oligomers up to  $\sim 750$  amu for aqueous methylglyoxal using LDI-MS.

#### **3.3.3 Role of NaCl from Aerosol-CIMS data**

Hemiacetal species have been observed by others to be present in aqueous methylglyoxal solutions in the absence of salts (Nemet et al., 2004). Aldol condensation was also predicted to be favorable in aqueous methylglyoxal solutions by Barsanti and Pankow (2005) and Krizner et al. (2009). Therefore, the observation of several common peaks in the spectra of the aqueous methylglyoxal control, methylglyoxal/NaCl, and methylglyoxal/ $(\text{NH}_4)_2\text{SO}_4$  is to be expected. Comparison of the aqueous methylglyoxal control and methylglyoxal/NaCl spectra suggests that NaCl may enhance the formation of hemiacetal species, which are not light-absorbing.

#### **3.4 Mechanism**

The evidence from our UV-Vis and Aerosol-CIMS studies together with our ab initio calculations points to aldol condensation as the mechanism for formation of light-absorbing products in this system. We observed mass spectra consistent with aldol addition and aldol condensation products, and these species were shown via our ab initio calculations to be consistent with the observed UV-Vis absorption spectra. The calculations of Barsanti and Pankow (2005) and Krizner et al. (2009) suggested that aldol condensation should be favorable for methylglyoxal in aerosols, and it has long been known that methylglyoxal undergoes aldol condensation in the presence of amino acids to form brown products (Enders and Sigurdsson, 1943).

The results of our UV-Vis studies indicate that the formation of light-absorbing products is enhanced by the presence of  $\text{NH}_4^+$  and  $\text{H}_3\text{O}^+$ . Our Aerosol-CIMS data also provides supporting evidence that the presence of  $\text{NH}_4^+$  increases the formation of aldol addition and condensation products.

$\text{H}_3\text{O}^+$  is a well-known catalyst for aldol condensation (Jang et al., 2002; Nozière and Esteve, 2007; Casale et al., 2007). Nozière and coworkers have recently shown that  $\text{NH}_4^+$  is a catalyst for aldol condensation of ketones or aldehydes (Nozière and Cordova, 2007). The most likely point of participation of both  $\text{NH}_4^+$  and  $\text{H}_3\text{O}^+$  in the aldol condensation mechanism is the initial step when the carbonyl is protonated before attack by the enol. A protonated carbonyl can also lead to a number of subsequent reactions besides aldol condensation, including hemiacetal formation or amine substitution (Nozière et al., 2009b). Two recent studies report the formation of C-N compounds by glyoxal when  $\text{NH}_4^+$  is present in the aqueous phase under acidic conditions (Nozière et al., 2009b; Galloway et al., 2009), and both propose mechanisms involving ammonia and iminium intermediates. The low pH in this study will result in low equilibrium  $\text{NH}_3$  concentrations. However, the protonation of a carbonyl by  $\text{NH}_4^+$  as proposed here and by Nozière et al. (2009b) would result in the generation of a short-lived  $\text{NH}_3$  molecule proximal to the reaction site. Nozière et al. (2009b) reported that the iminium pathway was active for glyoxal in ammonium-containing solutions down to pH 4.8 (the lowest pH studied).

### 3.5 Kinetics

The data in Fig. 3 demonstrate a linear dependence for the absorbance at 282 nm on initial methylglyoxal concentration and initial ammonium sulfate concentration, respectively, when pH=2. This is consistent with the protonation of methylglyoxal by ammonium being the rate-limiting step in the formation of light-absorbing dimers. The inverse dependence of product formation on pH is consistent with acid-catalyzed aldol condensation occurring in parallel with the ammonium-facilitated process. The following model can be used to describe this system:

$$\frac{d[\text{P}]}{dt} = k_{\text{A}}^{\text{II}}[\text{MG}][\text{NH}_4^+] + k_{\text{B}}^{\text{II}}[\text{MG}][\text{H}_3\text{O}^+] - \frac{d[\text{MG}]}{dt} \quad (7)$$

$$\frac{d[\text{NH}_4^+]}{dt} = -k_{\text{A}}^{\text{II}}[\text{MG}][\text{NH}_4^+] \quad (8)$$

$$\frac{d[\text{H}_3\text{O}^+]}{dt} = -k_{\text{B}}^{\text{II}}[\text{MG}][\text{H}_3\text{O}^+] \quad (9)$$

Here, MG represents methylglyoxal and P represents light-absorbing products. This model can be used to describe the kinetic data in Fig. 2 or the concentration-dependent data in Fig. 3. A fit to the data can yield the bimolecular rate constants  $k_{\text{A}}^{\text{II}}$  and  $k_{\text{B}}^{\text{II}}$  if the molar absorptivity of the absorbing species are known. Referring to the UV-Vis absorption data in Fig. 3b, and assuming that the species responsible for the observed absorption at 282 nm are dimers of methylglyoxal and therefore their maximum concentration in the solution is half the initial concentration of methylglyoxal, a lower

bound for the molar absorptivity of the products absorbing at 282 nm is  $\epsilon \geq 4938 \text{ L mol}^{-1} \text{ cm}^{-1}$ . We used POLYMATH 6.10 to numerically integrate Eqs. (7–9). We find that the data in Figs. 2–3 can be described by this model with  $k_{\text{A}}^{\text{II}} \leq 5 \times 10^{-6} \text{ M}^{-1} \text{ min}^{-1}$  and  $k_{\text{B}}^{\text{II}} \leq 10^{-3} \text{ M}^{-1} \text{ min}^{-1}$ . This is consistent with the value we find ( $k_{\text{A}}^{\text{II}} \leq 4.2(\pm 0.2) \times 10^{-6} \text{ min}^{-1} \text{ M}^{-1}$ ) if we assume pseudo-first-order conditions and perform a weighted linear least squares fit to the data in Fig. 3c according to:

$$[\text{P}] \propto [\text{NH}_4^+]_0 (1 - \exp(-k_{\text{A}}^{\text{II}}[\text{MG}]_0 t)) \quad (10)$$

Based on our Aerosol-CIMS/ $\text{I}^-$  data we estimated a lower bound for the production rate of the aldol addition and condensation products detected at 271.5 amu (ref. Table 1) to be  $\geq 10^{-3} \text{ M min}^{-1}$ . If protonation of the methylglyoxal monomer is the rate-limiting step for formation of these products Eq. (7) should apply. Aerosol particles will become concentrated relative to the atomizer solution as the 100% RH atomizer output equilibrates to 60% RH. Following Tang and Munkelwitz (1994), an ammonium sulfate concentration of ~65 wt%, or 14 M, will be reached at 60% RH. Assuming the same proportional increase in concentration for methylglyoxal and  $\text{H}_3\text{O}^+$  we find  $[\text{MG}]_0 = 7.32 \text{ M}$  and  $[\text{H}_3\text{O}^+]_0 = 0.045 \text{ M}$ . Applying Eq. (7) and the bimolecular rate constants we derived based on the UV-Vis data ( $k_{\text{A}}^{\text{II}} \leq 5 \times 10^{-6} \text{ M}^{-1} \text{ min}^{-1}$  and  $k_{\text{B}}^{\text{II}} \leq 10^{-3} \text{ M}^{-1} \text{ min}^{-1}$ ) we find that at these high salt concentrations  $k_{\text{A}}^{\text{II}}[\text{NH}_4^+][\text{MG}]$  exceeds  $k_{\text{B}}^{\text{II}}[\text{H}_3\text{O}^+][\text{MG}]$  by a factor of 3, allowing us to approximate the production rate by  $dP/dt \approx k_{\text{A}}^{\text{II}}[\text{NH}_4^+][\text{MG}]$ . Using this and the measured production rate of  $\geq 10^{-3} \text{ M min}^{-1}$  we find a lower bound of  $k_{\text{A}}^{\text{II}} \geq 5 \times 10^{-6} \text{ M}^{-1} \text{ min}^{-1}$ . Coupling this with the upper bound obtained using the UV-Vis data, we conclude that  $k_{\text{A}}^{\text{II}} \approx 5 \times 10^{-6} \text{ M}^{-1} \text{ min}^{-1}$ .

## 4 Conclusions and atmospheric implications

The results of this study show that the ammonium ion plays an active role in the chemistry of methylglyoxal in aqueous aerosol mimics. This chemistry represents a new potential pathway for heterogeneous SOA formation.

We have made tentative identifications of an organosulfate product and C-N containing species using Aerosol-CIMS. To our knowledge, organosulfate formation by methylglyoxal in ammonium sulfate aerosols has not been observed previously, although Liggio et al. (2005a, b) and Galloway et al. (2009) identified organosulfate products in ammonium sulfate aerosols exposed to gas-phase glyoxal. Organosulfates have been identified in ambient aerosol (Gao et al., 2006; Iinuma et al., 2007; Gómez-González et al., 2008; Surratt et al., 2007, 2008; Russell et al., 2009; Lukács et al., 2009). Lukács et al. (2009) observed that organosulfate mass concentrations were at a maximum for submicron aerosol size fractions, suggesting a link between organosulfate formation and heterogeneous SOA formation pathways. If C-N

species form in this system, this could contribute to the nitrogen-containing aerosol organics which have been observed in ambient aerosol (Denkenberger et al., 2007; Aiken et al., 2008; Lin et al., 2009; Gilardoni et al., 2009).

To our knowledge, the concentrations of the methylglyoxal reaction products we have proposed here have not been measured in atmospheric aerosol samples. Kawamura and coworkers have measured methylglyoxal monomer and related compounds (glyoxal, ketocarboxylic acids, and dicarboxylic acids) in ambient aerosols (Sempere and Kawamura, 1994; Kawamura et al., 1996; Kawamura and Yasui, 2005; Ho et al., 2007; Kundu et al., 2009). Methylglyoxal was found to comprise roughly 0.005–0.05% of aerosol mass in urban environments (Kawamura and Yasui, 2005; Ho et al., 2007). Assuming a particle density of  $1\text{ g cm}^{-3}$  this corresponds to an in-particle methylglyoxal concentration range of 0.7 mM to 7 mM.

A typical ammonium sulfate concentration in an aqueous atmospheric aerosol particle at 60% RH is  $\sim 65\text{ wt}\%$  (Tang and Munkelwitz, 1994), or 14 M, with  $0 \leq \text{pH} \leq 5$  (Keene et al., 2004; Zhang et al., 2007), resulting in pseudo-first-order rate coefficients of  $k_{\text{A}}^1 = 1.4 \times 10^{-4}\text{ min}^{-1}$  and  $10^{-8}\text{ min}^{-1} \leq k_{\text{B}}^1 \leq 10^{-3}\text{ min}^{-1}$  for the loss of methylglyoxal through reaction with  $\text{NH}_4^+$  and  $\text{H}_3\text{O}^+$ , respectively. Given an aerosol-phase methylglyoxal concentration of 7 mM, this corresponds to a production rate of  $10^{-6}\text{ M min}^{-1}$  (at  $\text{pH}=5$ ) to  $8 \times 10^{-6}\text{ M min}^{-1}$  (at  $\text{pH}=0$ ). Based on our reaction model this corresponds to 0.7 to 6 mM of light-absorbing products formed after 12 h (up to 86% conversion of methylglyoxal to products).

What we have observed for the methylglyoxal/ $(\text{NH}_4)_2\text{SO}_4$  system is another example of aerosol-phase chemistry which may increase the absorption index of atmospheric aerosols with increasing aerosol age. These results add to the growing body of evidence that SOA formation and aging may be a source of “brown carbon” in atmospheric aerosols. Brown carbon, including the products observed here, does not absorb as strongly as black carbon at high wavelengths ( $\sim 550\text{ nm}$  and higher) and therefore its contribution to aerosol absorption in this range may be minor in comparison (Andreae and Gelencsér, 2006). However, the absorption of UV radiation by brown carbon has the potential to reduce tropospheric  $\text{O}_3$  levels (Jacobson, 1999, 2002). Based on our calculated molar absorptivity of  $\epsilon_{282} \geq 4938\text{ L mol}^{-1}\text{ cm}^{-1}$  and our estimated production rate of 0.7 to 6 mM light-absorbing products formed after 12 h, we estimate that the contribution to the dimensionless absorption coefficient at 282 nm from methylglyoxal reaction products is  $A_{282,\text{MG}} = \lambda \epsilon_{282} / 4\pi \sim 10^{-5}$ . On a per-mole basis, the light-absorbing products observed here are stronger absorbers in the range 250–400 nm than pyruvic or oxalic acids (Lund Myhre and Nielsen, 2004) or the light-absorbing products of glyoxal in aqueous ammonium sulfate solutions observed by Shapiro et al. (2009).

Our observation of surface tension depression is consistent with observations of surface tension depression by HULIS in ambient aerosol samples (Kiss et al., 2005; Salma et al., 2006; Taraniuk et al., 2007; Asa-Awuku et al., 2008). Referring to Fig. 4, based on our estimated in-particle methylglyoxal concentration of 7 mM, and assuming that the particles are primarily composed of ammonium sulfate, this corresponds to surface tension depression of approximately 8% due to methylglyoxal in urban particles. We note that, since methylglyoxal will react in the particle to form potentially surface-active products, this value likely underestimates the total amount of surface tension depression associated with methylglyoxal uptake to the particle. Decreased aerosol surface tension may affect the cloud nucleation ability of the aerosol. The ability of an aerosol particle to activate at a given supersaturation condition depends on the amount of solute present in the particle (i.e. its dry diameter) and the surface tension of the droplet at the point of activation. The Kohler curve that describes this process is given by (Kohler, 1936; Seinfeld and Pandis, 1998):

$$s = \frac{A}{D_p} - \frac{B}{D_p^3} \quad (11)$$

with

$$A = \frac{4M_w\sigma}{RT\rho_w} \quad \text{and} \quad B = \frac{6n_sM_w}{\pi\rho_w} \quad (12)$$

where  $s$  is the supersaturation,  $D_p$  is the diameter of the aqueous droplet,  $M_w$  is the molecular weight of water and  $\rho_w$  is its density,  $R$  is the gas constant,  $T$  is temperature,  $\sigma$  is surface tension, and  $n_s$  is the number of moles of solute. Surface tension depression in aqueous aerosols by methylglyoxal SOA material could therefore result in increased CCN activation due to its effect on the parameter  $A$ . It has been suggested that this effect may be partially compensated for by the effect of surface-active organic solute partitioning from the bulk to the gas-aerosol interface, thereby reducing the bulk solute concentration (and the value of  $B$ ) (Sorjamaa et al., 2004). However, in a heterogeneous SOA formation scenario the bulk solute content of the particle is expected to be dominated by salt. Furthermore, in order to maintain Henry's law equilibrium, gas-phase methylglyoxal will continuously be taken up at the aerosol surface as it is consumed by particle-phase reactions. Therefore we assume here that the effect of methylglyoxal and its reaction products on equilibrium CCN activity is purely surface-tension based. For particles of a given size, this effect can be expressed as:

$$s_c^* = \left( \frac{\sigma}{\sigma_w} \right)^{3/2} s_c \quad (13)$$

where  $s_c^*$  is the critical supersaturation,  $\sigma_w$  and  $\sigma$  are the surface tension of water and the particle, respectively, and  $s_c$  is the critical supersaturation for a particle with the surface tension of water (Engelhart et al., 2008). Based on 7 mM

methylglyoxal in the particle, we estimate  $\sigma/\sigma_w \sim 1.01$ , compared to  $\sigma/\sigma_w=1.09$  for a saturated ammonium sulfate solution (see Fig. 4). Using Eq. (13), this corresponds to a critical supersaturation  $\sim 11\%$  lower than that of a pure ammonium sulfate particle. CCN activation measurements are planned in order to confirm this effect. We note that the relevant surface tension is that of the droplet at the moment of activation, at which point the surfactant concentration will be lower than that in the aqueous aerosol at lower relative humidities, especially for larger particles. A film of surface-active organics coating an aqueous particle may also affect the kinetics of particle equilibration with the surrounding water vapor, thereby affecting cloud droplet growth rate and cloud droplet number (Archer and La Mer, 1955; Rosano and La Mer, 1956; Chuang et al., 1997; Feingold and Chuang, 2002; Garland et al., 2005; Ruehl et al., 2009).

The small size, and thus high surface area-to-volume ratio of a submicron aerosol particle means that, compared to the bulk solutions used here, a greater fraction of the total surfactant molecules present in the aerosol will partition to the interface. This will effectively decrease surface coverage for a given surfactant concentration and increase the critical micelle concentration (CMC) (McNeill et al., 2006). Based on this effect, we would expect the minimum surface tension in an aerosol particle to be similar to what was observed here, but the plateau region of the surface tension curve may not be reached until higher methylglyoxal concentrations. However, this effect may be balanced by the fact that the small size of aerosol particles also leads to supersaturated salt concentrations which were not accessible in this study (Tang and Munkelwitz, 1994; Tang et al., 1997; Tang, 1997). The CMC lowering effect of the salt and the increased “salting-out” may counteract the size effect.

Kroll et al. (2005) reported negligible particle growth when ammonium sulfate particles were exposed to  $\sim 960$  ppb of methylglyoxal in aerosol chamber experiments on a timescale of several hours, and attributed this to the Henry's law coefficient of methylglyoxal, which is low relative to that of glyoxal (Betterton and Hoffmann, 1988; Zhou and Mopper, 1990). Surface film formation such as is suggested by our surface tension measurements, even at submonolayer coverages (i.e. concentrations below the CMC), can also inhibit the reactive uptake of gas-phase species into the aerosol (Folkers et al., 2003; Thornton and Abbatt, 2005; Anttila et al., 2006; McNeill et al., 2006, 2007; Stemmler et al., 2008). Film formation upon uptake of methylglyoxal to the aerosol could result in suppressed VOC uptake (and therefore suppressed SOA formation and particle growth).

Finally, we have demonstrated here that Aerosol-CIMS using  $\text{I}^-$  and  $\text{H}_3\text{O}^+(\text{H}_2\text{O})_n$  as the parent ions is suitable for the detection of the products of heterogeneous SOA formation by  $\alpha$ -dicarbonyls, and high molecular weight organics up to 759 amu. This technique can be extended to aerosol chamber studies and, when coupled with a suitable aerosol collection or concentration technique, field studies.

**Acknowledgements.** This work was funded by the NASA Tropospheric Chemistry program (grant NNX09AF26G), the NSF BRIGE program (grant EEC-0823847), and by a Columbia University Professional Schools Research Fellowship for V.F.M. The authors gratefully acknowledge the Koberstein group for use of the pendant drop tensiometer and for helpful discussions. N.S., A.N.S. and E.L.S. contributed equally to this work.

Edited by: M. Ammann

## References

- Adamson, A. W. and Gast, A. P.: Physical chemistry of surfaces, Wiley, New York, 1997.
- Aiken, A. C., DeCarlo, P. F., Kroll, J. H., Worsnop, D. R., Huffman, J. A., Docherty, K. S., Ulbrich, I. M., Mohr, C., Kimmel, J. R., Sueper, D., Sun, Y., Zhang, Q., Trimborn, A., Northway, M., Ziemann, P. J., Canagaratna, M. R., Onasch, T. B., Alfarra, M. R., Prevot, A. S. H., Dommen, J., Duplissy, J., Metzger, A., Baltensperger, U., and Jimenez, J. L.: O/C and OM/OC ratios of primary, secondary, and ambient organic aerosols with high-resolution time-of-flight aerosol mass spectrometry, *Environ. Sci. Technol.*, 42(12), 4478–4485, 2008.
- Altieri, K. E., Seitzinger, S. P., Carlton, A. G., Turpin, B. J., Klein, G. C., and Marshall, A. G.: Oligomers formed through in-cloud methylglyoxal reactions: Chemical composition, properties, and mechanisms investigated by ultra-high resolution FT-ICR mass spectrometry, *Atmos. Environ.*, 42(7), 1476–1490, 2008.
- Anastasiadis, S. H., Chen, J. K., Koberstein, J. T., Siegel, A. F., Sohn, J. E., and Emerson, J. A.: The Determination of Interfacial-Tension by Video Image-Processing of Pendant Fluid Drops, *J. Colloid Interface Sci.*, 119(1), 55–66, 1987.
- Andreae, M. O. and Gelencsér, A.: Black carbon or brown carbon? The nature of light-absorbing carbonaceous aerosols, *Atmos. Chem. Phys.*, 6, 3131–3148, 2006, <http://www.atmos-chem-phys.net/6/3131/2006/>.
- Anttila, T., Kiendler-Scharr, A., Tillman, R., and Mentel, T. F.: On the Reactive Uptake of Gaseous Compounds by Organic-Coated Aqueous Aerosols: Theoretical Analysis and Application to the Heterogeneous Hydrolysis of  $\text{N}_2\text{O}_5$ , *J. Phys. Chem. A.*, 110(35), 10435–10443, 2006.
- Archer, R. J. and La Mer, V. K.: The rate of evaporation of water through fatty acid monolayers, *J. Phys. Chem.*, 59, 200–208, 1955.
- Asa-Awuku, A., Sullivan, A. P., Hennigan, C. J., Weber, R. J., and Nenes, A.: Investigation of molar volume and surfactant characteristics of water-soluble organic compounds in biomass burning aerosol, *Atmos. Chem. Phys.*, 8, 799–812, 2008, <http://www.atmos-chem-phys.net/8/799/2008/>.
- Attygalle, A. B., Garcia-Rubio, S., Ta, J., and Meinwald, J.: Collisionally-induced dissociation mass spectra of organic sulfate anions, *J. Chem. Soc.-Perkin Trans.*, 2(4), 498–506, 2001.
- Barsanti, K. C. and Pankow, J. F.: Thermodynamics of the formation of atmospheric organic particulate matter by accretion reactions – 2. Dialdehydes, methylglyoxal, and diketones, *Atmos. Environ.*, 39(35), 6597–6607, 2005.
- Bayliss, N. S. and McRae, E. G.: Solvent Effects in the Spectra of Acetone, Crotonaldehyde, Nitromethane, and Nitrobenzene, *J. Phys. Chem.*, 58, 1006–1011, 1954.



- Betterton, E. A. and Hoffmann, M. R.: Henry Law Constants of Some Environmentally Important Aldehydes, *Environ. Sci. Technol.*, 22(12), 1415–1418, 1988.
- Blake, R. S., Monks, P. S., and Ellis, A. M.: Proton-Transfer Reaction Mass Spectrometry, *Chem. Rev.*, 109(3), 861–896, 2009.
- Bogan, M. J., Patton, E., Srivastava, A., Martin, S., Ferguson, D. P., Steele, P. T., Tobias, H. J., Gard, E. E., and Frank, M.: Online aerosol mass spectrometry of single micrometer-sized particles containing poly(ethylene glycol), *Rapid Comm. Mass. Spec.*, 21, 1214–1220, 2007.
- Canny, J.: A Computational Approach to Edge Detection, *IEEE Trans. Patt. Anal. Mach. Intell.*, 8, 679–714, 1986.
- Carlton, A. G., Turpin, B. J., Altieri, K. E., Seitzinger, S. P., Mathur, R., Roselle, S. J., and Weber, R. J.: CMAQ Model Performance Enhanced When In-Cloud Secondary Organic Aerosol is Included: Comparisons of Organic Carbon Predictions with Measurements, *Environ. Sci. Technol.*, 42(23), 8798–8802, 2008.
- Carlton, A. G., Turpin, B. J., Lim, H. J., Altieri, K. E., and Seitzinger, S.: Link between isoprene and secondary organic aerosol (SOA): Pyruvic acid oxidation yields low volatility organic acids in clouds, *Geophys. Res. Lett.*, 33(6), L06822, doi:10.1029/2005GL025374, 2006.
- Casale, M. T., Richman, A. R., Elrod, M. J., Garland, R. M., Beaver, M. R., and Tolbert, M. A.: Kinetics of acid-catalyzed aldol condensation reactions of aliphatic aldehydes, *Atmos. Environ.*, 41(29), 6212–6224, 2007.
- Chuang, P. Y., Charlson, R. J., and Seinfeld, J. H.: Kinetic limitations on droplet formation in clouds, *Nature*, 390(6660), 594–596, 1997.
- Cruz, C. N. and Pandis, S. N.: A study of the ability of pure secondary organic aerosol to act as cloud condensation nuclei, *Atmos. Environ.*, 31(15), 2205–2214, 1997.
- De Haan, D. O., Corrigan, A. L., Smith, K. W., Stroik, D. R., Turley, J. J., Lee, F. E., Tolbert, M. A., Jimenez, J. L., Cordova, K. E., and Ferrell, G. R.: Secondary Organic Aerosol-Forming Reactions of Glyoxal with Amino Acids, *Environ. Sci. Technol.*, 43(8), 2818–2824, 2009a.
- De Haan, D. O., Tolbert, M. A., and Jimenez, J. L.: Atmospheric condensed-phase reactions of glyoxal with methylamine, *Geophys. Res. Lett.*, 36, LL11819, doi:10.1029/2009GL037441, 2009b.
- Denkenberger, K. A., Moffet, R. C., Holecek, J. C., Rebotier, T. P., and Prather, K. A.: Real-time, single-particle measurements of oligomers in aged ambient aerosol particles, *Environ. Sci. Technol.*, 41(15), 5439–5446, 2007.
- Duplissy, J., Gysel, M., Alfarra, M. R., Dommen, J., Metzger, A., Prevot, A. S. H., Weingartner, E., Laaksonen, A., Raatikainen, T., Good, N., Turner, S. F., McFiggans, G., and Baltensperger, U.: Cloud forming potential of secondary organic aerosol under near atmospheric conditions, *Geophys. Res. Lett.*, 35, L03818, doi:10.1029/2007GL031075, 2008.
- El Haddad, I., Yao Liu, Nieto-Gligorovski, L., Michaud, V., Temime-Roussel, B., Quivet, E., Marchand, N., Sellegri, K., and Monod, A.: In-cloud processes of methacrolein under simulated conditions – Part 2: Formation of secondary organic aerosol, *Atmos. Chem. Phys.*, 9, 5107–5117, 2009, <http://www.atmos-chem-phys.net/9/5107/2009/>.
- Enders, C. and Sigurdsson, S.: The chemistry of humic acid formation under physiological conditions, *V. Announcement: The introductory phase of the humic acid formation. A aldol condensation from methylglyoxal*, *Ber. Dtsch. Chem. Ges.*, 76, 562–565, 1943.
- Engelhart, G. J., Asa-Awuku, A., Nenes, A., and Pandis, S. N.: CCN activity and droplet growth kinetics of fresh and aged monoterpene secondary organic aerosol, *Atmos. Chem. Phys.*, 8, 3937–3949, 2008, <http://www.atmos-chem-phys.net/8/3937/2008/>.
- Feingold, G. and Chuang, P. Y.: Analysis of the influence of film-forming compounds on droplet growth: Implications for cloud microphysical processes and climate, *J. Atmos. Sci.*, 59(12), 2006–2018, 2002.
- Folkers, M., Mentel, T. F., and Wahner, A.: Influence of an organic coating on the reactivity of aqueous aerosols probed by the heterogeneous hydrolysis of N<sub>2</sub>O<sub>5</sub>, *Geophys. Res. Lett.*, 30(12), 1644–1647, 2003.
- Fu, T. M., Jacob, D. J., and Heald, C. L.: Aqueous-phase reactive uptake of dicarbonyls as a source of organic aerosol over eastern North America, *Atmos. Environ.*, 43(10), 1814–1822, 2009.
- Galloway, M. M., Chhabra, P. S., Chan, A. W. H., Surratt, J. D., Flagan, R. C., Seinfeld, J. H., and Keutsch, F. N.: Glyoxal uptake on ammonium sulphate seed aerosol: reaction products and reversibility of uptake under dark and irradiated conditions, *Atmos. Chem. Phys.*, 9, 3331–3345, 2009, <http://www.atmos-chem-phys.net/9/3331/2009/>.
- Gao, S., Surratt, J. D., Knipping, E. M., Edgerton, E. S., Shahgholi, M., and Seinfeld, J. H.: Characterization of polar organic components in fine aerosols in the southeastern United States: Identity, origin, and evolution, *J. Geophys. Res.-Atmos.*, 111(D14), D14314, doi:10.1029/2005JD006601, 2006.
- Garland, R. M., Wise, M. E., Beaver, M. R., DeWitt, H. L., Aiken, A. C., Jimenez, J. L., and Tolbert, M. A.: Impact of palmitic acid coating on the water uptake and loss of ammonium sulfate particles, *Atmos. Chem. Phys.*, 5, 1951–1961, 2005, <http://www.atmos-chem-phys.net/5/1951/2005/>.
- Gilardoni, S., Liu, S., Takahama, S., Russell, L. M., Allan, J. D., Steinbrecher, R., Jimenez, J. L., De Carlo, P. F., Dunlea, E. J., and Baumgardner, D.: Characterization of organic ambient aerosol during MIRAGE 2006 on three platforms, *Atmos. Chem. Phys.*, 9, 5417–5432, 2009, <http://www.atmos-chem-phys.net/9/5417/2009/>.
- Gómez-González, Y., Surratt, J. D., Cuyckens, F., Szmigielski, R., Vermeylen, R., Jaoui, M., Lewandowski, M., Offenberg, J. H., Kleindienst, T. E., Edney, E. O., Blockhuys, F., Van Alsenoy, C., Maenhaut, W., and Claeys, M.: Characterization of organosulfates from the photooxidation of isoprene and unsaturated fatty acids in ambient aerosol using liquid chromatography/(-) electrospray ionization mass spectrometry, *J. Mass Spec.*, 43(3), 371–382, 2008.
- Grosjean, D., Williams, E. L., and Grosjean, E.: Atmospheric Chemistry of Isoprene and of its Carbonyl Products, *Environ. Sci. Technol.*, 27(5), 830–840, 1993.
- Hartz, K. E. H., Rosenorn, T., Ferchak, S. R., Raymond, T. M., Bilde, M., Donahue, N. M., and Pandis, S. N.: Cloud condensation nuclei activation of monoterpene and sesquiterpene secondary organic aerosol, *J. Geophys. Res.-Atmos.*, 110(D14), D14208, doi:10.1029/2004JD005754, 2005.
- Hearn, J. D., Lovett, A. J., and Smith, G. D.: Ozonolysis of oleic acid particles: evidence for a surface reaction and secondary

- reactions involving Criegee intermediates, *Phys. Chem. Chem. Phys.*, 7(3), 501–511, 2005.
- Hearn, J. D., Renbaum, L. H., Wang, X., and Smith, G. D.: Kinetics and Products from a reaction of Cl radicals with dioctyl sebacate (DOS) particles in O<sub>2</sub>: a model for radical-initiated oxidation of organic aerosols, *Phys. Chem. Chem. Phys.*, 9, 1–11, 2007.
- Hearn, J. D. and Smith, G. D.: A chemical ionization mass spectrometry method for the online analysis of organic aerosols, *Anal. Chem.*, 76(10), 2820–2826, 2004a.
- Hearn, J. D. and Smith, G. D.: Kinetics and product studies for ozonolysis reactions of organic particles using aerosol CIMS, *J. Phys. Chem. A*, 108(45), 10019–10029, 2004b.
- Hearn, J. D. and Smith, G. D.: Measuring rates of reaction in supercooled organic particles with implications for atmospheric aerosol, *Phys. Chem. Chem. Phys.*, 7(13), 2549–2551, 2005.
- Hearn, J. D. and Smith, G. D.: A mixed-phase relative rates technique for measuring aerosol reaction kinetics, *Geophys. Res. Lett.*, 33(17), L17805, doi:10.1029/2006GL026963, 2006a.
- Hearn, J. D. and Smith, G. D.: Reactions and mass spectra of complex particles using Aerosol CIMS, *Int. J. Mass Spec.*, 258(1–3), 95–103, 2006b.
- Hearn, J. D. and Smith, G. D.: Ozonolysis of Mixed Oleic Acid/*n*-Docosane Particles: The Roles of Phase, Morphology, and Metastable States, *J. Phys. Chem. A*, 111(43), 11059–11065, 2007.
- Ho, K. F., Cao, J. J., Lee, S. C., Kawamura, K., Zhang, R. J., Chow, J. C., and Watson, J. G.: Dicarboxylic acids, ketocarboxylic acids, and dicarbonyls in the urban atmosphere of China, *J. Geophys. Res.-Atmos.*, 112(D22), D22S27, doi:10.1029/2006JD008011, 2007.
- Iinuma, Y., Muller, C., Berndt, T., Boge, O., Claeys, M., and Herrmann, H.: Evidence for the existence of organosulfates from beta-pinene ozonolysis in ambient secondary organic aerosol, *Environ. Sci. Technol.*, 41(19), 6678–6683, 2007.
- International Critical Tables of Numerical Data, Physics, Chemistry, and Technology (1st Electronic Edition), edited by: Washburn, E. W., Knovel, Norwich, NY, 2003.
- Jacobson, M. Z.: Isolating nitrated and aromatic aerosols and nitrated aromatic gases as sources of ultraviolet light absorption, *J. Geophys. Res.-Atmos.*, 104(D3), 3527–3542, 1999.
- Jacobson, M. Z.: Control of fossil-fuel particulate black carbon and organic matter, possibly the most effective method of slowing global warming, *J. Geophys. Res.-Atmos.*, 107(D19), 4410, doi:10.1029/2001JD001376, 2002.
- Jang, M. S., Czoschke, N. M., Lee, S., and Kamens, R. M.: Heterogeneous atmospheric aerosol production by acid-catalyzed particle-phase reactions, *Science*, 298(5594), 814–817, 2002.
- Juza, J.: The pendant drop method of surface tension measurement: Equation interpolating the shape factor tables for several selected planes, *Czech. J. Phys.*, 47(3), 351–357, 1997.
- Kalberer, M., Paulsen, D., Sax, M., Steinbacher, M., Dommen, J., Prevot, A. S. H., Fisseha, R., Weingartner, E., Frankevich, V., Zenobi, R., and Baltensperger, U.: Identification of polymers as major components of atmospheric organic aerosols, *Science*, 303(5664), 1659–1662, 2004.
- Kawamura, K., Kasukabe, H., and Barrie, L. A.: Source and reaction pathways of dicarboxylic acids, ketoacids and dicarbonyls in arctic aerosols: One year of observations, *Atmos. Environ.*, 30(10–11), 1709–1722, 1996.
- Kawamura, K. and Yasui, O.: Diurnal changes in the distribution of dicarboxylic acids, ketocarboxylic acids and dicarbonyls in the urban Tokyo atmosphere, *Atmos. Environ.*, 39(10), 1945–1960, 2005.
- Keene, W. C., Pszenny, A. A. P., Maben, J. R., Stevenson, E., and Wall, A.: Closure evaluation of size-resolved aerosol pH in the New England coastal atmosphere during summer, *J. Geophys. Res.-Atmos.*, 109(D23), D23202, doi:10.1029/2004JD004801, 2004.
- Kendall, R. A., Dunning, T. H., and Harrison, R. J.: Electron affinities of the first-row atoms revisited. Systematic basis sets and wave functions., *J. Chem. Phys.*, 96(9), 6796–6806, 1992.
- King, S. M., Rosenoern, T., Shilling, J. E., Chen, Q., and Martin, S. T.: Cloud condensation nucleus activity of secondary organic aerosol particles mixed with sulfate, *Geophys. Res. Lett.*, 34(24), L24806, doi:10.1029/2007GL030390, 2007.
- King, S. M., Rosenoern, T., Shilling, J. E., Chen, Q., and Martin, S. T.: Increased cloud activation potential of secondary organic aerosol for atmospheric mass loadings, *Atmos. Chem. Phys.*, 9, 2959–2971, 2009, <http://www.atmos-chem-phys.net/9/2959/2009/>.
- Kiss, G., Tombacz, E., and Hansson, H. C.: Surface tension effects of humic-like substances in the aqueous extract of tropospheric fine aerosol, *J. Atmos. Chem.*, 50(3), 279–294, 2005.
- Kohler, H.: The nucleus in the growth of hygroscopic droplets, *Trans. Faraday Soc.*, 32, 1152–1161, 1936.
- Krizner, H. E., De Haan, D. O., and Kua, J.: Thermodynamics and Kinetics of Methylglyoxal Dimer Formation: A Computational Study, *J. Phys. Chem. A*, 113(25), 6994–7001, 2009.
- Kroll, J. H., Ng, N. L., Murphy, S. M., Varutbangkul, V., Flanagan, R. C., and Seinfeld, J. H.: Chamber studies of secondary organic aerosol growth by reactive uptake of simple carbonyl compounds, *J. Geophys. Res.-Atmos.*, 110(D23), D23207, doi:10.1029/2005JD006004, 2005.
- Kundu, S., Kawamura, K., Andreae, T. W., Hoffer, A., and Andreae, M. O.: Molecular distributions of dicarboxylic acids, ketocarboxylic acids and  $\alpha$ -dicarbonyls in biomass burning aerosols: implications for photochemical production and degradation in smoke layers, *Atmos. Chem. Phys. Discuss.*, 9, 19783–19815, 2009, <http://www.atmos-chem-phys-discuss.net/9/19783/2009/>.
- Lajohn, L. A., Christiansen, P. A., Ross, R. B., Atashroo, T., and Ermler, W. C.: Abinitio Relativistic Effective Potentials with Spin Orbit Operators .3. Rb Through Xe, *J. Chem. Phys.*, 87(5), 2812–2824, 1987.
- Li, Z. D., Williams, A. L., and Rood, M. J.: Influence of soluble surfactant properties on the activation of aerosol particles containing inorganic solute, *J. Atmos. Sci.*, 55(10), 1859–1866, 1998.
- Liggio, J., Li, S. M., and McLaren, R.: Reactive uptake of glyoxal by particulate matter, *J. Geophys. Res.-Atmos.*, 110(D10), D10304, doi:10.1029/2004JD005113, 2005.
- Lin, M., Walker, J., Geron, C., and Khlystov, A.: Organic nitrogen in PM<sub>2.5</sub> aerosol at a forest site in the Southeast US, *Atmos. Chem. Phys. Discuss.*, 9, 17157–17181, 2009, <http://www.atmos-chem-phys-discuss.net/9/17157/2009/>.
- Loeffer, K. W., Koehler, C. A., Paul, N. M., and De Haan, D. O.: Oligomer formation in evaporating aqueous glyoxal and methyl glyoxal solutions, *Environ. Sci. Technol.*, 40(20), 6318–6323, 2006.

- Lund Myhre, C. E. and Nielsen, C. J.: Optical properties in the UV and visible spectral region of organic acids relevant to tropospheric aerosols, *Atmos. Chem. Phys.*, 4, 1759–1769, 2004, <http://www.atmos-chem-phys.net/4/1759/2004/>.
- Lukács, H., Gelencsér, A., Hoffer, A., Kiss, G., Horváth, K., and Hartyáni, Z.: Quantitative assessment of organosulfates in size-segregated rural fine aerosol, *Atmos. Chem. Phys.*, 9, 231–238, 2009, <http://www.atmos-chem-phys.net/9/231/2009/>.
- Matićević, E. and Pethica, B. A.: The properties of ionized monolayers, Part 1. Sodium dodecyl sulfate at the air/water interface, *Trans. Faraday Soc.*, 54, 1383–1389, 1958.
- McNeill, V. F., Wolfe, G. M., and Thornton, J. A.: The Oxidation of Oleate in Submicron Aqueous Salt Aerosols: Evidence of a Surface Process, *J. Phys. Chem. A*, 111, 1073–1083, 2007.
- McNeill, V. F., Yatavelli, R. L. N., Thornton, J. A., Stipe, C. B., and Landgrebe, O.: Heterogeneous OH oxidation of palmitic acid in single component and internally mixed aerosol particles: vaporization and the role of particle phase, *Atmos. Chem. Phys.*, 8, 5465–5476, 2008, <http://www.atmos-chem-phys.net/8/5465/2008/>.
- McNeill, V. F., Patterson, J., Wolfe, G. M., and Thornton, J. A.: The effect of varying levels of surfactant on the reactive uptake of N<sub>2</sub>O<sub>5</sub> to aqueous aerosol, *Atmos. Chem. Phys.*, 6, 1635–1644, 2006, <http://www.atmos-chem-phys.net/6/1635/2006/>.
- Meller, R., Raber, W., Crowley, J. N., Jenkin, M. E., and Moortgat, G. K.: The UV-Visible Absorption-Spectrum of Methylglyoxal, *J. Photochem. Photobiol. A*, 62(2), 163–171, 1991.
- Michaud, V., El Haddad, I., Yao Liu, Sellegri, K., Laj, P., Villani, P., Picard, D., Marchand, N., and Monod, A.: In-cloud processes of methacrolein under simulated conditions – Part 3: Hygroscopic and volatility properties of the formed secondary organic aerosol, *Atmos. Chem. Phys.*, 9, 5119–5130, 2009, <http://www.atmos-chem-phys.net/9/5119/2009/>.
- Muller, P.: Glossary of Terms Used in Physical Organic Chemistry (IUPAC Recommendations 1994), *Pure Appl. Chem.*, 66(5), 1077–1184, 1994.
- Nemet, I., Vikić-Topić, D., and Varga-Defterdarović, L.: Spectroscopic studies of methylglyoxal in water and dimethylsulfoxide, *Bioorg. Chem.*, 32(6), 560–570, 2004.
- Nozière, B. and Cordova, A.: A novel catalyst for aldol condensation reaction, WO2009045156, 2007.
- Nozière, B., Dziedzic, P., and Cordova, A.: Formation of secondary light-absorbing “fulvic-like” oligomers: A common process in aqueous and ionic atmospheric particles?, *Geophys. Res. Lett.*, 34(21), L21812, doi:10.1029/2007GL031300, 2007.
- Nozière, B., Dziedzic, P., and Córdoba, A.: Common inorganic ions are efficient catalysts for organic reactions in atmospheric aerosols and other natural environments, *Atmos. Chem. Phys. Discuss.*, 9, 1–21, 2009a, <http://www.atmos-chem-phys-discuss.net/9/1/2009/>.
- Nozière, B., Dziedzic, P., and Cordova, A.: Products and Kinetics of the Liquid-Phase Reaction of Glyoxal Catalyzed by Ammonium Ions (NH<sub>4</sub><sup>+</sup>), *J. Phys. Chem. A*, 113(1), 231–237, 2009b.
- Nozière, B. and Esteve, W.: Light-absorbing aldol condensation products in acidic aerosols: Spectra, kinetics, and contribution to the absorption index, *Atmos. Environ.*, 41(6), 1150–1163, 2007.
- Paulsen, D., Dommen, J., Kalberer, M., Prevot, A. S. H., Richter, R., Sax, M., Steinbacher, M., Weingartner, E., and Baltensperger, U.: Secondary organic aerosol formation by irradiation of 1,3,5-trimethylbenzene-NO<sub>x</sub>-H<sub>2</sub>O in a new reaction chamber for atmospheric chemistry and physics, *Environ. Sci. Technol.*, 39(8), 2668–2678, 2005.
- Rosano, H. L. and La Mer, V. K.: The Rate of Evaporation of Water Through Monolayers of Esters, Acids, and Alcohols, *J. Phys. Chem.*, 60, 348–353, 1956.
- Ruehl, C. R., Chuang, P. Y., and Nenes, A.: Distinct CCN activation kinetics above the marine boundary layer along the California coast, *Geophys. Res. Lett.*, 36, L15814, doi:10.1029/2009GL038839, 2009.
- Russell, L. M., Takahama, S., Liu, S., Hawkins, L. N., Covert, D. S., Quinn, P. K., and Bates, T. S.: Oxygenated fraction and mass of organic aerosol from direct emission and atmospheric processing measured on the R/V Ronald Brown during TEX-AQS/GoMACCS 2006, *J. Geophys. Res.-Atmos.*, 114, D00F05, doi:10.1029/2008JD011275, 2009.
- Saathoff, H., Naumann, K. H., Schnaiter, M., Schöck, W., Mohler, O., Schurath, U., Weingartner, E., Gysel, M., and Baltensperger, U.: Coating of soot and (NH<sub>4</sub>)<sub>2</sub>SO<sub>4</sub> particles by ozonolysis products of alpha-pinene, *J. Aerosol Sci.*, 34(10), 1297–1321, 2003.
- Salma, I., Ocskay, R., Varga, I., and Maenhaut, W.: Surface tension of atmospheric humic-like substances in connection with relaxation, dilution, and solution pH, *J. Geophys. Res.-Atmos.*, 111(D23), D23205, doi:10.1029/2005JD007015, 2006.
- Seinfeld, J. H. and Pandis, S. N.: *Atmospheric Chemistry and Physics: from air pollution to climate change*, Wiley, New York, 1998.
- Sempere, R. and Kawamura, K.: Comparative Distributions of Dicarboxylic-Acids and Related Polar Compounds in Snow Rain and Aerosols from Urban Atmosphere, *Atmos. Environ.*, 28(3), 449–459, 1994.
- Setschenow, J. Z.: Über Die Konstitution der Salzsäuren auf Grund ihres Verhaltens zu Kohlensäure, *Z. Physik. Chem.*, 4, 117–125, 1889.
- Shapiro, E. L., Szprengiel, J., Sareen, N., Jen, C. N., Giordano, M. R., and McNeill, V. F.: Light-absorbing secondary organic material formed by glyoxal in aqueous aerosol mimics, *Atmos. Chem. Phys.*, 9, 2289–2300, 2009, <http://www.atmos-chem-phys.net/9/2289/2009/>.
- Shulman, M. L., Jacobson, M. C., Carlson, R. J., Synovec, R. E., and Young, T. E.: Dissolution behavior and surface tension effects of organic compounds in nucleating cloud droplets, *Geophys. Res. Lett.*, 23(3), 277–280, 1996.
- Skoog, D. A., Holler, F. J., and Nieman, T. A.: *Principles of Instrumental Analysis*, Saunders College Publishing, New York, 1997.
- Smith, D. F., Kleindienst, T. E., and McIver, C. D.: Primary product distributions from the reaction of OH with m-, p-xylene, 1,2,4- and 1,3,5-trimethylbenzene, *J. Atmos. Chem.*, 34(3), 339–364, 1999.
- Sorjamaa, R., Svenningsson, B., Raatikainen, T., Henning, S., Bilde, M., and Laaksonen, A.: The role of surfactants in Köhler theory reconsidered, *Atmos. Chem. Phys.*, 4, 2107–2117, 2004, <http://www.atmos-chem-phys.net/4/2107/2004/>.
- Stemmler, K., Vlasenko, A., Guimbaud, C., and Ammann, M.: The effect of fatty acid surfactants on the uptake of nitric acid to deliquesced NaCl aerosol, *Atmos. Chem. Phys.*, 8, 5127–5141,

- 2008,  
<http://www.atmos-chem-phys.net/8/5127/2008/>.
- Surratt, J. D., Gómez-González, Y., Chan, A. W. H., Vermeylen, R., Shahgholi, M., Kleindienst, T. E., Edney, E. O., Offenberg, J. H., Lewandowski, M., Jaoui, M., Maenhaut, W., Claeys, M., Flagan, R. C., and Seinfeld, J. H.: Organosulfate formation in biogenic secondary organic aerosol, *J. Phys. Chem. A*, 112(36), 8345–8378, 2008.
- Surratt, J. D., Kroll, J. H., Kleindienst, T. E., Edney, E. O., Claeys, M., Sorooshian, A., Ng, N. L., Offenberg, J. H., Lewandowski, M., Jaoui, M., Flagan, R. C., and Seinfeld, J. H.: Evidence for organosulfates in secondary organic aerosol, *Environ. Sci. Technol.*, 41(2), 517–527, 2007.
- Tang, I. N.: Thermodynamic and optical properties of mixed-salt aerosols of atmospheric importance, *J. Geophys. Res.-Atmos.*, 102(D2), 1883–1893, 1997.
- Tang, I. N. and Munkelwitz, H. R.: Water Activities, Densities, and Refractive-Indexes of Aqueous Sulfates and Sodium-Nitrate Droplets of Atmospheric Importance, *J. Geophys. Res.-Atmos.*, 99(D9), 18801–18808, 1994.
- Tang, I. N., Tridico, A. C., and Fung, K. H.: Thermodynamic and optical properties of sea salt aerosols, *J. Geophys. Res.-Atmos.*, 102(D19), 23269–23275, 1997.
- Taraniuk, I., Graber, E. R., Kostinski, A., and Rudich, Y.: Surfactant properties of atmospheric and model humic-like substances (HULIS), *Geophys. Res. Lett.*, 34(16), L16807, doi:10.1029/2007GL029576, 2007.
- Thornberry, T., Murphy, D. M., Thomson, D. S., de Gouw, J. A., Warneke, C., Bates, T. S., Quinn, P. K., and Coffman, D.: Measurement of Aerosol Organic Compounds Using a Novel Collection/Thermal-Desorption PTR-ITMS Instrument, *Aerosol Sci. Technol.*, 43(5), 486–501, 2009.
- Thornton, J. A. and Abbatt, J. P. D.: N<sub>2</sub>O<sub>5</sub> Reaction on Sub-micron Sea Salt Aerosol: Effect of Surface Active Organics, *J. Phys. Chem. A*, 109(44), 10004–10012, 2005.
- Tuazon, E. C., Macleod, H., Atkinson, R., and Carter, W. P. L.: Alpha-Dicarbonyl Yields from the Nox-Air Photooxidations of A Series of Aromatic-Hydrocarbons in Air, *Environ. Sci. Technol.*, 20(4), 383–387, 1986.
- Volkamer, R., Jimenez, J. L., San Martini, F., Dzepina, K., Zhang, Q., Salcedo, D., Molina, L. T., Worsnop, D. R., and Molina, M. J.: Secondary organic aerosol formation from anthropogenic air pollution: Rapid and higher than expected, *Geophys. Res. Lett.*, 33(17), L17811, doi:10.1029/2006GL026899, 2006.
- Volkamer, R., San Martini, F., Molina, L. T., Salcedo, D., Jimenez, J. L., and Molina, M. J.: A missing sink for gas-phase glyoxal in Mexico City: Formation of secondary organic aerosol, *Geophys. Res. Lett.*, 34, L19807, doi:10.1029/2007GL030752, 2007.
- Volkamer, R., Ziemann, P. J., and Molina, M. J.: Secondary Organic Aerosol Formation from Acetylene (C<sub>2</sub>H<sub>2</sub>): seed effect on SOA yields due to organic photochemistry in the aerosol aqueous phase, *Atmos. Chem. Phys.*, 9, 1907–1928, 2009,  
<http://www.atmos-chem-phys.net/9/1907/2009/>.
- Zhang, Q., Jimenez, J. L., Worsnop, D. R., and Canagaratna, M.: A case study of urban particle acidity and its influence on secondary organic aerosol, *Environ. Sci. Technol.*, 41(9), 3213–3219, 2007.
- Zhao, J., Levitt, N. P., Zhang, R. Y., and Chen, J. M.: Heterogeneous reactions of methylglyoxal in acidic media: Implications for secondary organic aerosol formation, *Environ. Sci. Technol.*, 40(24), 7682–7687, 2006.
- Zhou, X. L. and Mopper, K.: Apparent Partition-Coefficients of 15 Carbonyl-Compounds Between Air and Seawater and Between Air and Fresh-Water – Implications for Air Sea Exchange, *Environ. Sci. Technol.*, 24(12), 1864–1869, 1990.